Infrared studies of the superconducting energy gap and normal-state dynamics of the high-T_c superconductor $YBa_2Cu_3O_7$

Z. Schlesinger, R. T. Collins, F. Holtzberg, C. Feild, G. Koren, and A. Gupta
IBM Thomas J. Watson Research Center, Yorktown Heights, New York 10598
(Received 26 October 1989; revised manuscript received 2 April 1990)

A detailed study of infrared properties (reflectivity, conductivity, and dielectric response), emphasizing reproducible results from fully oxygenated $YBa_2Cu_3O_7$ crystals ($T_c \simeq 93$ K) and films, is presented. The extrapolated values of $\sigma_1(\omega)$ at low frequency are roughly consistent with the measured temperature-dependent dc resistivity. Although not well understood, this infrared conductivity can be interpreted in terms of a frequency-dependent scattering rate of $\sim kT + \hbar\omega$, with a low-frequency mass enhancement of roughly 2 to 4 associated with a carrier-spin related interaction. Infrared measurements polarized along the c axis suggest a conductivity anisotropy of roughly 40:1 near T_c in the normal state. In the superconducting state an energy scale of $2\Delta_c \simeq 3kT_c$ is suggested by c-axis polarized measurements, while a much larger characteristic energy of $2\Delta_{a\text{-}b} \simeq 8kT_c$ is evident in the (a-b)-plane conductivity. From the area missing from the conductivity up to this very large gap, a reasonable estimate ($\simeq 1700$ Å) for the (a-b)-plane penetration depth is obtained. Evidence for non-BCS temperature dependence, strong pair breaking scattering, and possible fluctuation effects is discussed. A comparison to infrared data from $Bi_2Sr_2CaCu_2O_{8-y}$ shows a similarly large energy scale, $2\Delta_{a\text{-}b} \simeq 8kT_c$; for the cubic $Ba_{0.6}K_{0.4}BiO_3$ superconductor a more conventional energy scale, $2\Delta \simeq 4kT_c$ is observed. The unusually large energy scale obtained from the (a-b)-plane measurements of the layered cuprates lies far beyond the range of previously studied superconducting energy gaps ($2\Delta \simeq 3$ to $5kT_c$).

I. INTRODUCTION

In the phenomenology of superconductivity, the energy gap, or, more generally, the spectrum of excitations in the superconducting state, plays a central role. Because of the fundamental relationship between the gap and the density of thermally excited quasiparticles in the superconducting state, knowledge of the symmetry, temperature dependence, and magnitude of the gap is generally sufficient to explain the behavior of the specific heat, nuclear relaxation, penetration depth, microwave absorption, and other low-energy properties in the superconducting state. Beginning with the pioneering work of Glover and Tinkham[1] and of Giaver,[2] both infrared[3–7] and tunnelling spectroscopies[8] have provided the most fundamental and versatile probes of the superconducting energy gap. Tunneling probes the single-particle density of states, which is gapped at Δ in a conventional superconductor; while infrared measures the conductivity, which has a gap at the threshold for pair excitations, 2Δ. In the oxides tunneling is more difficult than in conventional superconductors due both to the short coherence length, and the difficulty of preparing well-characterized junctions at oxide surfaces. Infrared measurements, on the other hand, probe more deeply than tunnelling ($\simeq 1500$ Å), and actually become significantly less difficult as the frequency range of interest, which tends to scale with T_c, becomes higher. In this article we present infrared measurements of the recently discovered high-T_c cuprate superconductors,[9,10] and discuss their implications regarding the nature of the excitation spectrum in both the superconducting and normal states. Work on the fully oxygenated $YBa_2Cu_3O_7$ is emphasized since it is with this stoichiometric compound that we obtain our most reproducible results.

Infrared measurements on the layered cuprates began with studies of ceramic samples[11–24] in which the presence of a large, uncontrolled anisotropy was extremely problematic. These measurements were later essentially superseded by studies of crystalline materials,[25–39] in which the response associated with the in-plane and out-of-plane directions could be clearly identified. In the following discussion a brief review of the use of infrared measurements to address the nature of the superconducting energy gap and the normal-state dynamics in the layered cuprates is presented.

From the infrared data on ceramics, estimates of a reduced energy gap in the range $2\Delta/kT_c \simeq 2$ to 3.5 were widely reported (see Refs. 11–17). At that time one of the puzzles associated with the high-T_c field was why the infrared gap appeared to be small compared both to the BCS value ($3.5kT_c$), and estimates of the gap based on tunnelling (see Refs. 14 and 22). Based on very elementary considerations associated with the normal-state conductivity anisotropy, we proposed that the infrared gap measurement on unoriented polycrystalline samples should be dominated by contributions with the electric field perpendicular to the Cu-O plane, and quite insensi-

tive to the (a-b)-plane gap.[22] Recent c-axis polarized measurements on both $YBa_2Cu_3O_7$ (Ref. 36) and $La_{2-x}Sr_xCuO_4$ (Ref. 39) are quite consistent with this proposal, as discussed in Sec. III E of this article.

In the first infrared measurement of crystalline $YBa_2Cu_3O_7$,[25] both the absolute (a-b)-plane reflectivity at room temperature, and the ratio of the reflectivity in the superconducting state to that in the normal state (R_s/R_n) were reported. Based on the reflectivity ratio, which exhibits a peak at about 500 cm^{-1} ($\simeq$720 K), an energy gap of $\sim 8kT_c$ was inferred for the a-b plane.[25,28] These reflectivity ratios, and hence the assignment of the gap energy, appear to have been quite accurate and are in good agreement with subsequent work. The high degree of reproducibility of the ratio measurement is due to the fact that only relative accuracy is required. The absolute reflectivities reported in the early studies,[25,28] were too low due to our inability to calibrate the absolute reflectivity accurately (i.e., establish what is 100%), particularly with the early "mosaic samples," which consisted of pieces of several small crystals mounted together.[25,28,29] More recent measurement of larger, individual (although microtwinned) crystals and films, now show an acceptable level of reproducibility in the absolute reflectivity, as discussed in this article. We emphasize that these differences in absolute reflectivity are not indicative of sample quality.

As noted above, the original inference of the $2\Delta_{a-b} \simeq 8kT_c$ gap was based on the measurement of the ratio, R_s/R_n, of the reflectivity in the superconducting state to that in the normal state.[25] The emphasis on ratios over absolute quantities in infrared gap measurements dates to the work of Glover and Tinkham.[1] Virtually all subsequent infrared gap measurements (see Refs. 3–7) have also used ratios of superconducting and normal-state properties to determine the energy of the gap, and have not attempted to show directly that the absorption below the gap vanishes in the superconducting state as the temperature (T) goes to 0. Recently it has been proposed that the correct way to extract a superconducting gap from infrared data is to establish the frequency at which the reflectivity first deviates from 100%.[30] In an ideal measurement of a BCS (isotropic) superconductor this criterion, and the older one of inferring the energy gap from the peak in a measured ratio will lead to identical results. In the layered Cu-O superconductors, however, very different conclusions have been reached using these two methods. Applying the 100% criterion to some of their oxygen reduced $YBa_2Cu_3O_{7-x}$ crystals, Thomas *et al.*[30] have reported evidence for a BCS size gap ($2\Delta \simeq 3.5kT_c$), while application of this criterion to fully-oxygenated $YBa_2Cu_3O_7$ has lead to the conclusion that there is either a much smaller gap, i.e., $2\Delta/kT_c \lesssim 2$,[35] or no discernible gap.[29] In our own work we have used temperature-dependent measurements in the vicinity of T_c to associate the $\sim 8kT_c$ energy scale with the transition to superconductivity.[25,36] Our conclusions regarding its relevance to the superconducting state thus do not depend on the unresolved question of whether or not the reflectivity of an ideal cuprate superconductor should be 100% up to $\simeq 8kT_c$. In this article we examine in more detail the gaplike, and very unconventional nature of this $\simeq 8kT_c$ superconducting state feature.

Regarding the possibility of a BCS size gap in the layered copper-oxides, our results from $YBa_2Cu_3O_7$ show little evidence for this in either the reflectivity ratios or the absolute reflectivity of the a-b plane. We find it very difficult to determine a specific frequency at which the absolute (a-b)-plane reflectivity reaches 100% in our samples, although reflectivities in excess of 99.5% are observed below about 150 cm^{-2}, i.e., $2\Delta \lesssim 2kT_c$. At the present level of accuracy, such a high reflectivity cannot be conclusively distinguished from 100%. Our measurements with the electric field perpendicular to the planes, on the other hand, do show evidence for a characteristic energy scale of roughly $2\Delta_c \simeq 3kT_c$ associated with the c-axis response.[36]

We note that some of the recent discussions regarding the inference of a gap energy from infrared measurements, parallel an earlier controversy that followed the original report of a superconducting energy gap in Pb.[1,40,41] Recent statement to the effect that infrared measurements cannot be interpreted as evidence for a superconducting gap in the cuprates, are closely related to arguments advanced earlier by Forrester[40] and responded to by Tinkham and Glover.[41]

Turning now to the normal state, infrared reflectivity data from ceramic samples were originally analyzed in a way that gave a strong excitonic feature in the infrared conductivity at about 0.4 eV.[18–20] It has been subsequently argued that this excitonic peak was an artifact associated with an incomplete treatment of anisotropy in the polycrystalline data analysis.[22,23] We find these arguments to be compelling. Infrared measurements on $La_{2-x}Sr_xCuO_4$ (Ref. 27) and $YBa_2Cu_3O_7$ (Refs. 25 and 26) crystals show substantial conductivity extending into the mid-infrared range ($\sim$0.5 eV), but no sharp excitonic peak in $\sigma_1(\omega)$ as reported for the ceramics (Refs. 18–20).

Early efforts to fit the room temperature (a-b)-plane reflectivity to a Drude model required a very large scattering rate,[25–27] which, as pointed out by Kamaras *et al.*,[24] would imply an unrealistically short mean-free path, and does not allow a reasonable explanation of the temperature dependence of the dc conductivity. The behavior of the dc conductivity and the far-infrared conductivity are, of course, fundamentally connected. In fact, the problem of understanding the temperature dependence of the dc conductivity is subsumed by the larger problem of understanding the temperature and frequency dependence of the infrared conductivity, which are themselves interrelated. Infrared measurements have explored these relationships, revealing a highly temperature- and frequency-dependent, low-frequency infrared conductivity.[29–31] Extrapolations of the infrared conductivity to $\omega=0$ give values in reasonable correspondence with dc results. At finite ω the infrared conductivity falls much less rapidly with frequency than would be expected for an ordinary metal.[29–31] Attempts to understand the conductivity have been based on both spin interaction[30,31] and charge excitation pictures,[29] as discussed in Sec. IV A. In the former case the carriers are

dressed by spin-related excitations, resulting in a reduced scattering rate and an enhanced mass at low frequency. In the latter case the free-carrier contribution to $\sigma(\omega)$ is supplemented by a strong mid-infrared charge excitation.

Most of the infrared data addressing these questions is from $YBa_2Cu_3O_7$ crystals, which, in addition to the CuO_2 planes, contain CuO chains oriented along the b direction. Presumably the chains are inessential to the superconductivity and it is the CuO_2-plane response that is of major interest; however, the high-T_c crystals tend to be heavily twinned in the a-b plane, hence it is not easy to separate the chain and plane contributions to $\sigma(\omega)$. This uncertainty in the origin of $\sigma(\omega)$ contributes to the ambiguity in the analysis of the normal-state dynamics, as discussed in Sec. IV A. The extent to which the chains actually contribute to the conductivity in the infrared is not well known, however, recent polarized measurements on small untwinned crystals suggest a large chain-related contribution[37] to $\sigma(\omega)$, which could account for some of the broad background conductivity observed in infrared measurements. Definitively separating the conductivity of $YBa_2Cu_3O_7$ into chain and plane contributions is an important goal of future work.

In spite of these uncertainties associated with its complex structure, $YBa_2Cu_3O_7$ has been the system of choice for infrared studies. $YBa_2Cu_3O_7$ is the only known stoichiometric high-T_c superconductor, and is the material for which the best crystals and films have been available. Flux-grown crystals and laser ablation films of the fully oxygenated $YBa_2Cu_3O_7$ have optically smooth surfaces and appear to have a high degree of electronic homogeneity (as evidenced, for example, by the very large and sharp specific-heat jump at T_c seen in the $YBa_2Cu_3O_7$ crystals[42–44]]. Both of these properties are crucially important for reliable infrared measurements.

In this article we examine the infrared reflectivity and conductivity of $YBa_2Cu_3O_7$ in both the normal and superconducting states. We primarily emphasize data from the fully-oxygenated $YBa_2Cu_3O_7$ ($T_c \simeq 92$ K), although some comparison is made to data from reduced-T_c $YBa_2Cu_3O_{7-x}$ crystals, as well as $Bi_2Sr_2CaCu_2O_{8-y}$ and $Ba_{0.6}K_{0.4}BiO_3$. We find that there is very good reproducibility in the absolute reflectivities and conductivities for the fully oxygenated $YBa_2Cu_3O_7$ ($T_c \gtrsim 92$ K), as well as in the reflectivity ratios (R_s/R_n), and show that the important energy scale for the a-b plane is 500 cm^{-1} ($\simeq 700$ K $\simeq 8kT_c$). The correspondence between our infrared data and the measured low-temperature penetration depth[45,46] is demonstrated by calculating the penetration depth from the area missing from the superconducting state conductivity up to above $\simeq 8kT_c$. The unconventional temperature dependence of this $8kT_c$ gaplike feature, as well as possible evidence for unusual fluctuation effects in the infrared conductivity above T_c are discussed in Sec. IV B. We also consider the possibility of a smaller gap (as suggested based on results from O deficient material) but conclude that there is very little evidence for this in the (a-b)-plane reflectivity of $YBa_2Cu_3O_7$ at the present time. Results from other gap sensitive probes, including specific heat,[42–44] tunneling,[47–54] photoelectron spectroscopy,[55–57] Raman scattering,[58–62] and nuclear resonance,[63–69] are discussed in Sec. IV B 6. For the most part, results from these techniques are consistent with the very large gap we have reported from infrared measurements.[25,36] In Sec. V, we compare the infrared results for $YBa_2Cu_3O_7$ to the analogous results from the cubic Bi-O superconductor, $Ba_{0.6}K_{0.4}BiO_3$.[70] The ratio of the reflectivity in the superconducting state to that in the normal state for each of these oxide superconductors is presented in Fig. 1. This measured ratio, R_s/R_n, is qualitatively very similar for these two systems, however, the same analysis applied to both sets of data leads to the inference of a conventional energy scale ($2\Delta \simeq 4kT_c$) for $Ba_{0.6}K_{0.4}BiO_3$, and a very unconventional energy scale, ($2\Delta_{a\text{-}b} \simeq 8kT_c$), for the a-b plane of $YBa_2Cu_3O_7$.

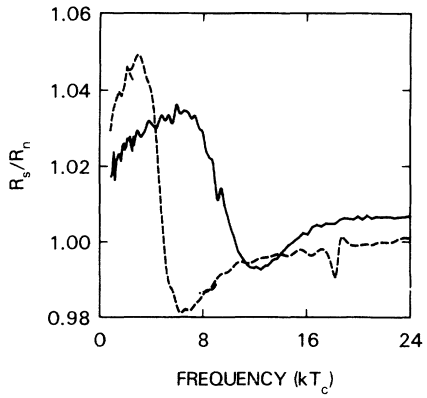

FIG. 1. Ratio of the reflectivity in the superconducting state to that in the normal state is shown for $Ba_{0.6}K_{0.4}BiO_3$ and for (the a-b plane of) $YBa_2Cu_3O_7$. R_s/R_n is plotted as a function of energy in units of kT_c, where $T_c = 29$ K for the $Ba_{0.6}K_{0.4}BiO_3$, and $T_c = 92$ K for the $YBa_2Cu_3O_7$. From the frequency of the peak in each plot, reduced energy scales of $2\Delta \simeq 4kT_c$ and $2\Delta_{a\text{-}b} \simeq 8kT_c$ are, respectively, inferred. (The structure at about $18kT_c$ in the dashed curve has an instrumental origin.)

II. EXPERIMENTAL PROCEDURES

A. Sample preparation

The highly anisotropic structural and transport properties of the Cu-O superconductors make oriented samples a necessity in infrared studies of these materials. In this paper we discuss results from both crystalline samples and oriented thin films of $YBa_2Cu_3O_{7-x}$, emphasizing results from fully oxygenated $YBa_2Cu_3O_7$ samples. The crystals were grown from a flux as previously described.[71] Following growth, they were annealed for 10 days at 420 °C in flowing oxygen after which they consistently exhibited extremely sharp superconducting transitions with widths less than 0.3 K and $T_c \simeq 93$ K as measured by ac susceptibility and shown in Fig. 2(a). In general, the crystals were highly twinned [predominantly

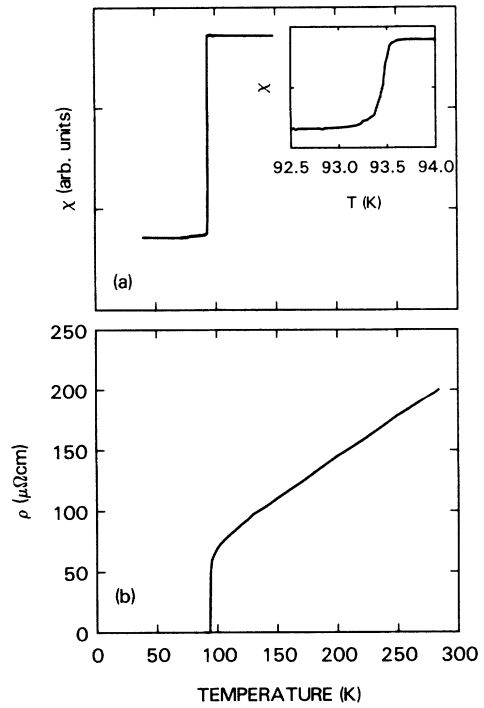

FIG. 2. (a) ac susceptibility (χ) as a function of temperature for a $YBa_2Cu_3O_7$ crystal. The inset shows χ in the region of the transition. The high-transition temperature and narrow-transition width are characteristic of the fully oxygenated $YBa_2Cu_3O_7$ crystals used in this work. (b) Resistivity as a function of temperature for the $YBa_2Cu_3O_7$ film used in this study. The film is $\simeq 0.4$-μ thick, and is oriented with the c axis perpendicular to the surface.

along (110) boundaries] within the a-b plane. Their geometry was platelike with typical dimensions of 1–2 mm along the a and b axis and 50 μm along the c axis. The (a-b)-plane measurements were made on individual crystals. Both "*as*-annealed" sample surfaces and surfaces which were mechanically polished with diamond paste to an 0.5 μm grit size were studied. As discussed below, polishing did not have a measurable effect on the infrared properties of the surface. This is presumably related to the deep penetration depth for infrared radiation (~ 1500 Å) in $YBa_2Cu_3O_7$.

To obtain sufficient area for measurements with the electric field along the c axis, a stack of $\simeq 12$ crystals was used. The stack was potted in epoxy and polished to obtain a flat surface; the fill fraction of crystal within epoxy was about 50%. given the larger penetration depth for the c axis relative to the a-b plane, polishing can be expected to have even less of an effect along this direction.

Crystals with reduced transition temperatures were also prepared for study. This was accomplished either by the removal of oxygen in a subsequent anneal or by doping with impurity atoms such as Mg. The crystals with reduced oxygen concentration generally showed broader transitions (5–15 K wide), suggesting considerable inhomogeneity in oxygen content or location. The impurities in the Mg-doped samples were introduced indirectly through growth in an MgO crucible, thus, the Mg concentration is at the saturation value for the growth temperature and is not readily variable. The Mg-doped samples typically have a transition temperature of $\simeq 80$ K with a width of about 1 K. The reduced oxygen content crystals with $T_c \sim 60$ K have a typical transition width of 10 K.

The films were deposited by the laser ablation technique onto (100) $SrTiO_3$ substrates at 730 °C in 0.2 Torr oxygen ambient.[72,73] Fully oxygenated films were obtained by adding 1 atm of oxygen at the end of the deposition experiment and cooling down slowly. They typically had a zero-resistance transition temperature of 92 K and a 1-K transition width [Fig. 2(b)]. Films with lower transition temperatures (40–60 K) were prepared by the use of lower oxygen pressures of about 0.5–1 Torr during the cooling procedure. All films are microtwinned on a very fine scale in the a-b plane. Fiml thicknesses range from about 200 Å to 0.5 μm. In reflectivity measurements on films, features associated with the substrate tend to appear if the film is not substantially thicker than the infrared penetration depth (~ 1500 Å). In this study we discuss reflectivity results on the thicker films (0.4 μm), for which these substrate related effects are not observable.

B. Infrared measurements techniques

The infrared reflectivity spectra presented in the article were acquired at near normal incidence ($\simeq 12°$) using a scanning interferometer. A number of different sources, beamsplitters, detectors, and windows were used to obtain data from 50–12 000 cm^{-1}. At low frequencies a Si bolometer mounted on a diamond substrate was used in conjunction with Mylar beam splitters, a Hg arc source, and high-density white polyethylene windows on the sample and detector dewars. To obtain high bolometer sensitivity, cold filters and apertures mounted on a filter wheel inside the bolometer dewar were used to restrict the amount of background blackbody radiation reaching the bolometer. A high-frequency cutoff of about 700 cm^{-1} is set by the white polyethylene windows.

To reach higher frequencies the white polyethylene windows are replaced by KRS5 windows, which transmit from about 200 cm^{-1} up to beyond 20 000 cm^{-1}. Data was obtained below 5000 cm^{-1} using both bolometric detection (200–5000 cm^{-1}) and a HgCdTe photoconductive detector (800–5000 cm^{-1}) with a CsI beamsplitter, and glowbar source. To obtain data at higher frequencies, photovoltaic detectors [InSb (2500–8000 cm^{-1}), Ge ($\gtrsim 5500$ cm^{-1}), and Si ($\gtrsim 8700$)], a quartz beamsplitter, and tungsten lamp source were used. There was substantial overlap in the range of frequencies covered with each of these combinations and the coincidence of the spectra was usually better than 1%, which allowed an entire spectrum from 50–12 000 cm^{-1} to be determined with a high degree of confidence regarding the absence of systematic errors.

Samples were mounted in a circulating Helium cold finger cryostat on a sliding sample holder. An evaporated Au mirror, which was used as a reference, was mounted in close proximity to the sample. A manipulator al-

lowed the sample holder to be moved so that either the sample or the reference could be positioned in the infrared beam as the measurements were made. A comparison of Au-to-Au and Brass-to-Au reflectivity ratios indicated an accuracy of about 1% in the absolute reflectivity obtained in this manner. Since the absorptivity of Au is less than this, no correction was made for residual absorption in the reference. The absolute accuracy of our normalization was primarily limited by our ability to align the samples and Au mirror surfaces parallel to one another. The relative accuracy of our measurement once the sample and mirror were fixed in position is even better than the absolute accuracy, thus we are able to observe very small ($\sim 0.1\%$) temperature-dependent changes in the reflectivity.

C. Kramers-Kronig transform

While much can be learned from direct inspection of reflectivity curves, the infrared conductivity $\sigma(\omega)$ is a more fundamental quantity from which to analyze the infrared response of the oxide superconductors. To obtain $\sigma(\omega)$ one applies a Kramers-Kronig transform to the reflectivity $R(\omega)$, which yields the phase shift $\theta(\omega)$. From $\theta(\omega)$ and $R(\omega)$ the real and imaginary parts of $\sigma(\omega)$ are calculated at each frequency. (For a discussion of Kramers-Kronig transforms see, for example, Ref. 74.) Formally, the phase-shift integral requires a knowledge of the reflectivity at all frequencies. In practice, one obtains the reflectivity over as wide a frequency range as possible and then terminates the transform by extrapolating the reflectivity to frequencies above and below the range of the available measurements. This extrapolation must be done with considerable care since significant contributions to $\theta(\omega)$ can come from the reflectance at frequencies well removed from the region of interest.

In the present work we have experimental with a variety of terminations both at the high- and low-frequency ends of our measurement range. Regarding the low-frequency termination, we find that the conductivities obtained using various extrapolations for the reflectivity at low ω differ primarily only in the region of the extrapolation. The conductivity at frequencies for which there is actual data is not effected significantly by the choice of low-frequency termination. In this paper we have extended the transform to lower frequencies by attaching a reflectivity of the Hagens-Rubens form $[(1-R) \propto \sqrt{\omega}]$ to our spectra.

The high-frequency termination appears to be more crucial. Although most choices for the termination give the same qualitative spectral shape in the region of the data, the choice of the high-frequency termination can have a large effect on the overall magnitude of the conductivity in the infrared region. This primarily effects estimates of the integrated strength of the conductivity, which are used in sum-rule arguments. In the present work potential problems related to the high-frequency termination are avoided by appending to our data the reflectivity spectra of Tajima *et al.*,[34] which extend up to 280 000 cm^{-1} (34 eV). In that data very large, broad peaks in $\sigma_1(\omega)$ are present near 8 eV ($\sim 60\,000$ cm^{-1}) and 15 eV ($\sim 125\,000$ cm^{-1}). These peaks have an enormous oscillator strength relative to the infrared conductivity (about 50 times larger), and appear to tail gradually into the infrared region with no clear low-frequency cutoff. These tails may account for part of the mid-infrared conductivity (at ~ 5000 cm^{-1}) discussed below. Above about 200 000 cm^{-1}, the reflectivity given by Tajima *et al.*[34] varies as $1/\omega^4$, which is the free-electron asymptotic limit. We terminate the transform above 280 000 cm^{-1} by assuming the $1/\omega^4$ form of the reflectivity continues above this frequency. We also find that changing the reflectivity above 280 000 cm^{-1} does not have a significant effect on the conductivity at infrared frequencies, and therefore believe this approach gives an accurate determination of the conductivity below 12 000 cm^{-1} for $YBa_2Cu_3O_7$.

III. RESULTS

A. (a-b)-plane normal state

In Fig. 3(a) the measured (a-b)-plane reflectivity of fully oxygenated $YBa_2Cu_3O_7$ is shown up to 10 000 cm^{-1} for $T=100$ K (solid line) and $T=250$ K (dashed line). As the temperature is lowered from 250 to 100 K, the infrared reflectivity increases almost uniformly over a broad frequency range up to ~ 8000 cm^{-1}, as previously reported.[31] This has important implications for infrared sum rules, as discussed in Sec. IV A. From the Kramers-Kronig transform of this reflectivity data, along with other data[34] extending up to 280 000 cm^{-1} (35 eV), the real and imaginary parts of $\epsilon(\omega)$ are obtained. The terminations used in the transform, as well as the importance of terminating the data appropriately, are discussed in Sec. II. From the imaginary part of $\varepsilon(\omega)$, one can obtain the real part of the conductivity, $\sigma_1(\omega)$, using $\sigma_1(\omega)=\omega\epsilon_2(\omega)/4\pi$. $\sigma_1(\omega)$ and $\epsilon_1(\omega)$ are plotted as a function of frequency in Figs. 3(b) and 3(c), respectively. The infrared conductivity, $\sigma_1(\omega)$, in Fig. 3(b) has a peak at the origin, which grows and sharpens as the temperature is lowered from 250 to 100 K. Above about 500 cm^{-1} $\sigma_{1n}(\omega)$ decreases gradually and monotonically with increasing frequency. A background conductivity at a level of about 500–1500 ($\Omega^{-1}\,cm^{-1}$ extends throughout of the infrared. This mid-infrared conductivity is quite reproducible in $YBa_2Cu_3O_7$, however, determining if this conductivity is present in all Cu-O superconductors, remains a key issue. In Sec. IV several possible explanations for this conductivity and their significance are discussed.

The dielectric function, $\epsilon_1(\omega)$, is negative at low frequencies and crosses zero at about 8000 cm^{-1}, as shown in Fig. 3(c). The frequency of this plasma edge is about a factor of 3–5 lower than in a typical metal such as Ag.[74] Recent polarized data from untwinned domains of a $YBa_2Cu_3O_7$ crystal report the resolution of this plasma edge into two distinct edges at ~ 7000 cm^{-1} and ~ 9000 cm^{-1} associated with the a and b crystal axes, respectively.[37] It has been suggested that an (a-b)-plane plasma edge is present in $YBa_2Cu_3O_7$ in a frequency range close to the energy gap, making it virtually impossible to deter-

mine an energy gap from infrared data.[29] As shown here and in other work,[31,34–37] this is not the case; the $(a\text{-}b)$-plane plasma edge lies well above the frequency range relevant for energy gap measurement.

In Fig. 4(a) the temperature dependence of the reflectivity in the normal state is shown in more detail for $\omega \lesssim 2000$ cm^{-1} and $T=250$, 200, 150, and 105 K. The reflectivity [Fig. 4(a)] increases rather uniformly as the temperature is lowered from 250 to 105 K. To avoid confusion, $\sigma_1(\omega)$ and $\epsilon_1(\omega)$ are shown only at the endpoints of this temperature sequence in Figs. 4(b) and 4(c). The observation that a displacement of $\epsilon_1(\omega)$ accompanies the growth of the peak in $\sigma_1(\omega)$ at low frequency is a reflection of the Kramers-Kronig relationship between these two quantities. At $T=105$ K the extrapolated peak value of $\sigma_1(\omega)$ at $\omega=0$ is between 15 000 and 20 000 Ω^{-1} cm^{-1}, and the half-width of this peak is roughly 150 cm^{-1} (i.e., $\sim 2kT_c$). Extrapolated values of the dc resistivity, discussed in Sec. IV A, are plotted as a function of temperature, in the inset to Fig. 4(b).

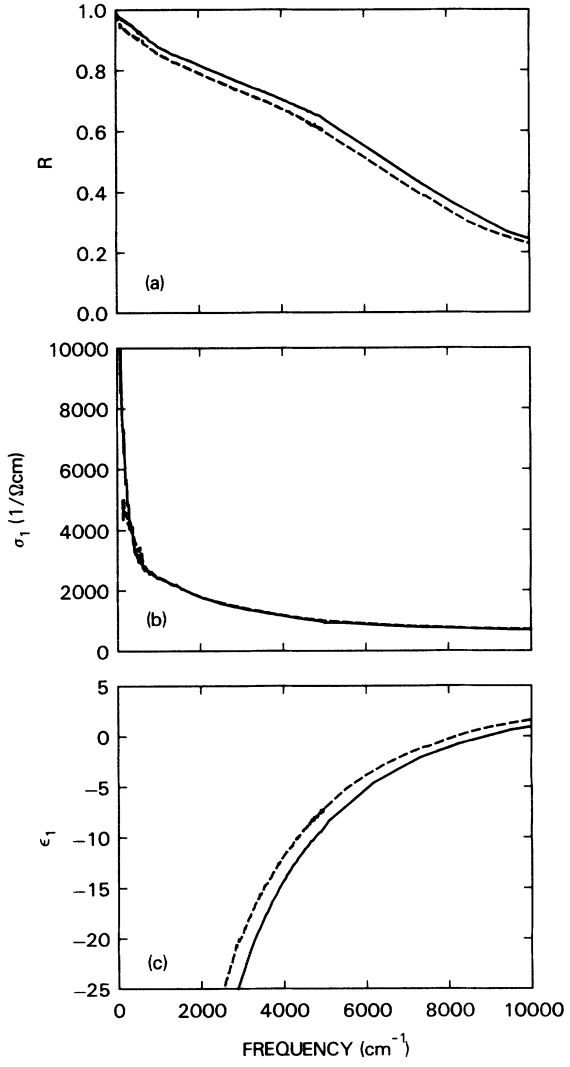

FIG. 3. Reflectivity at 250 K (dashed curve) and 105 K (solid curve) for the a-b plane of a $YBa_2Cu_3O_7$ crystal ($T_c \simeq 93$ K). The real part of the conductivity, $\sigma_1(\omega)$, and the real part of the dielectric function, $\epsilon_1(\omega)$, obtained from a Kramers-Kronig transform of the reflectivity, are shown in (b) and (c), respectively.

B. (a-b)-plane superconducting state

The uniform pattern of temperature dependence established in the normal state (Fig. 4) gives way to qualitatively different behavior in the superconducting state (Fig. 5). R, $\sigma_1(\omega)$, and $\epsilon_1(\omega)$ are shown at three temperatures in Fig. 5: one well into the normal state (150 K),

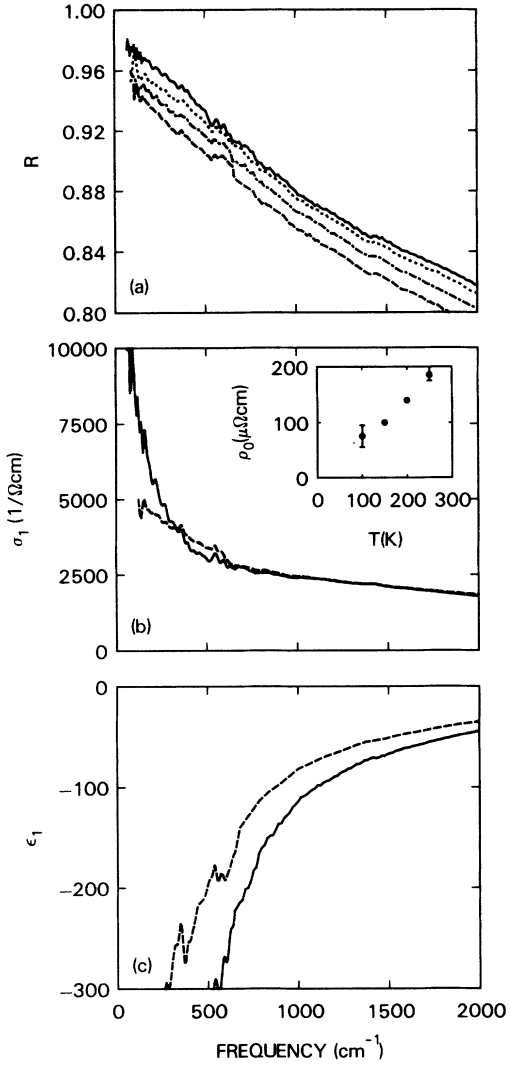

FIG. 4. (a) The normal state $(a\text{-}b)$-plane reflectivity of a $YBa_2Cu_3O_7$ crystal at 105 K (solid curve), 150 K (dotted curve), 200 K (dotted-dashed curve), and 250 K (dashed curve) is shown. (b) The real part of the conductivity, $\sigma_1(\omega)$, at 105 K (solid curve) and 250 K (dashed curve) obtained from the Kramers-Kronig transform of the reflectivity data in (a) are shown. The temperature dependence of the dc resistivity, obtained from an extrapolation to $\omega=0$, is shown in the inset. (c) $\epsilon_1(\omega)$ is shown at $T=105$ K (solid curve) and 250 K (dashed curve). The structures at about 350 and 500 cm^{-1} are phonon related.

one just above the transition (105 K), and one in the superconducting state (45 K). These quantities are essentially independent of temperature below about 55 K, thus the 45-K spectra are representative of the superconducting state at low temperature. The superconducting reflectivity is quite high for $\omega \lesssim 500$ cm^{-1}, drops rapidly between 500 and 800 cm^{-1}, and lies below the normal-state reflectivity in the vicinity of 800 cm^{-1}. Correspondingly, the superconducting-state conductivity is depressed for $\omega \lesssim 500$ cm^{-1}, and increases rapidly above this frequency, colaescing with $\sigma_{1n}(\omega)$ near about 900 cm^{-1}. In the frequency range between about 500 and 800 cm^{-1}, we also observe that $\epsilon_{1s}(\omega)$ crosses above $\epsilon_{1n}(\omega)$. This crossover of $\epsilon_{1s}(\omega)$ is directly related to both the rapid rise of $\sigma_{1s}(\omega)$ between 500 and 800 cm^{-1}, and the lower value of the reflectivity in the superconducting state relative to that in the normal state near 800 cm^{-1}.

The depression of $\sigma_{1s}(\omega)$ below 500 cm^{-1} and the rapid return to normalcy between 500 and 800 cm^{-1}, suggest a depression of the single-particle density of states near E_f, with a pair excitation threshold near 500 cm^{-1}. Between about 150 and 500 cm^{-1}, $\sigma_{1s}(\omega)$ is slowly varying with a value between 1000 and 2000 Ω^{-1} cm^{-1}. Various possible sources of this conductivity at low T below 500 cm^{-1} are discussed in Sec. IV B, where it is noted that this level is comparable to a recently reported experimental estimate of the chain-related contribution to $\sigma_1(\omega)$ in this frequency range.[37]

Below 150 cm^{-1} the uncertainty in $\sigma_{1s}(\omega)$ becomes quite large. The tendency of the absolute uncertainty in $\sigma_{1s}(\omega)$ to increase at low frequency is an intrinsic problem in infrared measurements of bulk (i.e., thick) samples. Although not rigorous, one can view the uncertainty in $\sigma_{1s}(\omega)$ as resulting from the low-ω divergence in the noise-to-signal ratio for the absorptivity, $A=1-R$, as R approaches unity. Looking in more detail, the absolute error in $\sigma_{1s}(\omega)$ is related to the magnitude of $\epsilon_{1s}(\omega)$, which diverges like $1/\omega^2$. This leads to a rapidly increasing uncertainty in $\sigma_{1s}(\omega)$ at low frequency. The problem is further exacerbated by the experimental tendency of the noise in R to increase at low ω (due both to decreasing source intensity and the increase in cavity resonance problems at long wavelength). One can "solve" these

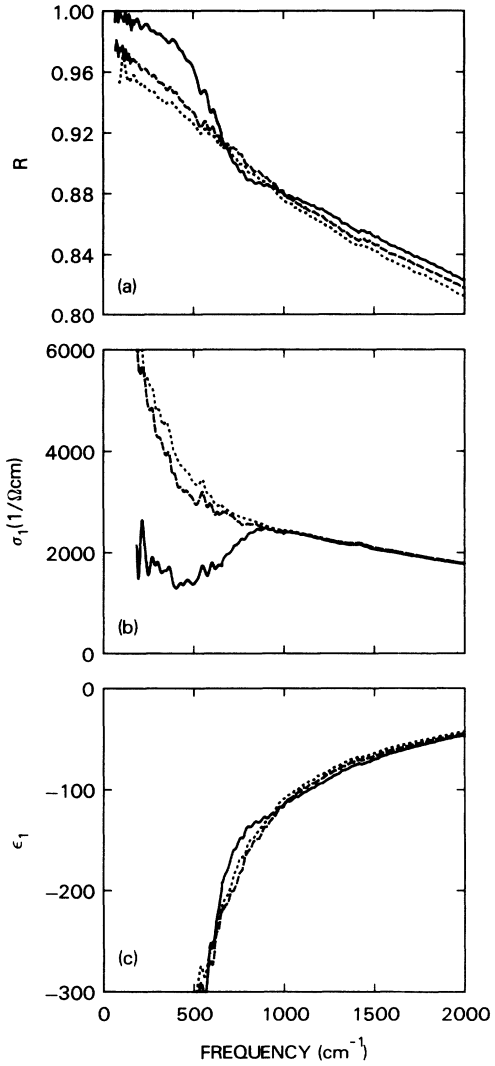

FIG. 5. (a) a-b reflectivity in the superconducting state at 45 K (solid line) and in the normal state at 105 K (dashed line) and 150 K (dotted line) for a $YBa_2Cu_3O_7$ crystal with $T_c \simeq 93$ K is shown. The corresponding conductivity, $\sigma_1(\omega)$, and $\epsilon_1(\omega)$ are shown in (b) and (c). There is an enhancement of the reflectivity and a gaplike depression of the conductivity in the superconducting state for $\omega \lesssim 500$ cm^{-1}.

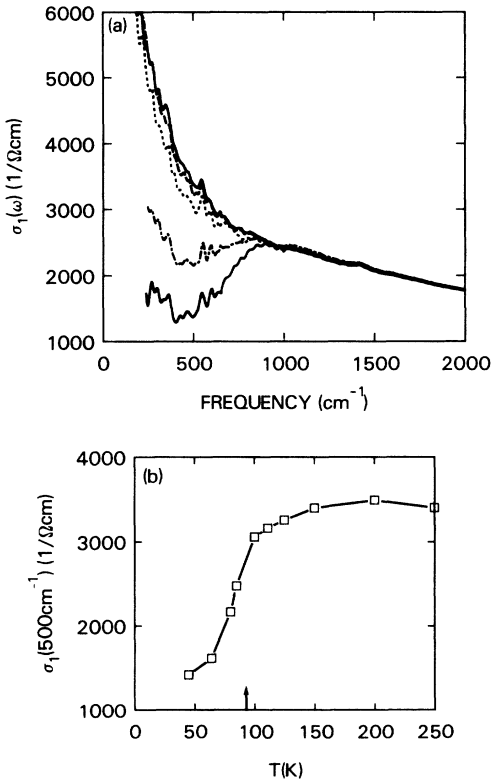

FIG. 6. (a) The real part of the (a-b)-plane conductivity of a $YBa_2Cu_3O_7$ crystal is shown for $T=45$ K (solid curve), 80 K (dotted-dashed curve), 105 K (dotted curve), 125 K (dashed curve), and 150 K (solid curve), respectively. In (b) the temperature dependence of the conductivity at 500 cm^{-1}, which is quite rapid just below T_c, is shown.

problems by setting the reflectivity exactly equal to unity below a particular frequency, thus cutting off the growing noise envelope in $\sigma_{1s}(\omega)$ at a chosen frequency below which $\sigma_{1s}(\omega)$ is set to 0. This approach leads to a prominent feature in the conductivity at the cutoff frequency for which there is no evidence in the data. In the present work, we have instead terminated each plot of $\sigma_{1s}(\omega)$ at about the frequency where its uncertainty exceeds ~ 1000 $\Omega^{-1}\,\mathrm{cm}^{-1}$.

The temperature dependence of the conductivity is examined more closely in Fig. 6(a), where spectra at $T=45$, 80, 105, 125, and 150 K are shown. In the vicinity of 500 cm^{-1} the conductivity begins to drop quite rapidly below T_c, and by 80 K (dotted-dashed curve) lies well below the normal state curves. Below 50 K the reflectivity and conductivity are essentially independent of temperature. In Fig. 6(b) the conductivity at 500 cm^{-1} is shown as a function of temperature. The rapid drop of σ_1 (500) just below T_c reinforces the fundamental relationship between the suppression of $\sigma_1(\omega)$ and the transition to the superconducting state. It also provides a means to observe the transition into the superconducting state which is analogous to microwave or dc conductivity measurements as a function of temperature.

The corresponding temperature dependence of the reflectivity ratios, $R(T)/R$ (150 K) is shown in Fig. 7. Above T_c these reflectivity ratios are primarily flat lines, reflecting the uncomplicated temperature dependence of the normal state, however, below T_c a characteristic "S shape" emerges with a peak in R_s/R_n at $\omega \simeq 500$ cm^{-1}. The inset of Fig. 7 shows the difference between the reflectivity at 400 and 800 cm^{-1} as a function of temperature, which grows rapidly just below T_c. In Fig. 8(a) the ratio of the conductivity at a temperature T to that at 150 K is shown for $T=45$ K (solid curve), 80 K (dashed curve), and 105 K (dotted curve).

In these Figs. 7 and 8 one observes that the amplitude of the gaplike feature associated with the transition to superconductivity is very strongly temperature dependent near T_c. In contrast, the characteristic frequency of this feature does not appear to change substantially even in the vicinity of T_c, as illustrated in Fig. 8(b). [For Fig. 8(b) the characteristic frequency is obtained by extrapolating the conductivity ratio above the gap down to the level of the minimum in σ_s/σ_n.] The lower dotted curve shows a BCS temperature dependence for $T_c=93$ K. [It is inappropriate to scale the BCS curve in a manner which fails to preserve the relationship $2\Delta(0)=3.52kT_c$, since the physics of gap collapse and the magnitude of the gap are intimately related.] It is clear that the temperature dependence does not follow a BCS curve, but rather that the gap remains quite large up to as close to T_c as we can measure. This unusual temperature dependence, the large magnitude of the gap, and the short coherence lengths in the cuprate superconductors may be related, as discussed in Sec. IV B 4.

An additional unconventional aspect of the infrared data can be seen in the conductivity ratios shown in Fig. 8(a). Even in the 105-K spectrum, there is a minimum in the vicinity of 300–500 cm^{-1} which is reminiscent of the prominent gaplike feature that is present at lower temperatures. These data suggest the possibility of fluctuation effects which are not describable in the conventional Aslamasov-Larkin formulation, as also discussed in Sec. IV B 4.

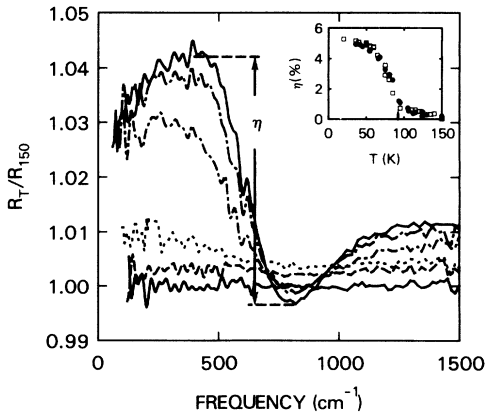

FIG. 7. The ratio of the (*a*-*b*)-plane reflectivity at a temperature T to that at 150 K is shown for $T=45$ K (solid curve), 65 K (dotted-dashed curve), 80 K (dotted-dashed curve), 105 K (dotted curve), 125 K (dashed curve), and 150 K (solid curve). In the inset the difference between the value of this ratio at 400 and at 800 cm^{-1} is plotted as a function of temperature, illustrating the fundamental relationship between the $\simeq 8kT_c$ reflectivity enhancement and the transition to the superconducting state (at $T_c \simeq 93$ K).

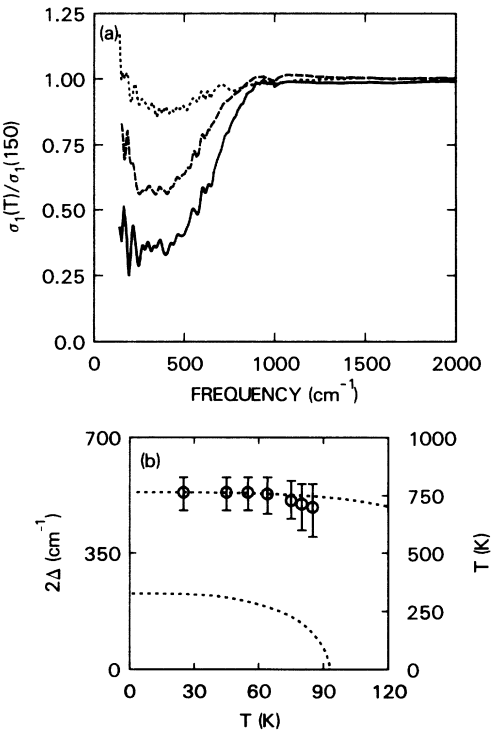

FIG. 8. (a) The ratio of the real part of the (*a*-*b*)-plane conductivity at a temperature T to that at 150 K is shown for $T=45$ K (solid curve), 80 K (dashed curve), and 105 K (dotted curve) for a $YBa_2Cu_3O_7$ crystal with $T_c \simeq 93$ K. In (b) a characteristic gap frequency is plotted as a function of temperature. The lower dotted curve shows the BCS (mean-field) temperature dependence for $T_c=93$ K.

C. Reduced T_c samples

For reduced T_c $YBa_2Cu_3O_{7-x}$ samples a distinction between the temperature dependence in the normal and superconducting states has not been established.[30] The gaps which have been reported for these materials are based on attempts to establish a frequency at which the reflectivity first departs from unity,[30] rather than from detailed studies of the temperature dependencies similar to those present here. Our own measurements of reduced-T_c samples show either a small change or no noticeable change in the infrared temperature dependence near T_c. For a Mg-doped sample, with $T_c \simeq 80$ K, we observe a reflectivity enhancement below $\simeq 600$ cm^{-1} which correlates with T_c and is very similar to that seen in the 93-K material, however, the amplitude of the enhancement (R_s/R_n) is about a factor of 3 less than for the fully oxygenated $YBa_2Cu_3O_7$ (even though the absolute reflectivity is lower in the Mg-doped sample). This observation raises the possibility that this feature of the data may be absent entirely in $YBa_2Cu_3O_{7-x}$ samples with lower T_c. We note that it is difficult to observe a definite change at T_c in the temperature dependencies of other physical properties (such as specific heat[44] and nuclear quadrupole relaxation rate[65–67] in oxygen depleted $YBa_2Cu_3O_{7-x}$, although the same quantities exhibit sharp breaks at T_c in fully oxygenated material.

It has been suggested that a "knee" near 500 cm^{-1} in the reflectivity of $YBa_2Cu_3O_{7-x}$ with reduced T_c is related to the 500-cm^{-1} gap feature we find in fully oxygenated $YBa_2Cu_3O_7$.[75] The possible nature of this relationship, if one exists, is unclear. We have looked for a 500-cm^{-1} reflectance edge in the normal state of our reduced-T_c samples, but find that the presence of infrared active (a-b)-plane phonons, which tend to become more prominent in lower-T_c crystals because of reduced electronic screening, makes it difficult to tell whether such a "knee" is present, or if in the absence of phonons the reflectivity would drop smoothly throughout this frequency range. There appear to be substantial differences between the infrared properties of $YBa_2Cu_3O_{7-x}$ with $T_c = 93$ K and various reduced-T_c variations. At present these differences are not well understood.

D. Reproducibility

As noted above, obtaining an acceptable level of reproducibility in the absolute reflectivity has been much more difficult than with the reflectivity ratios. In this section we examine the level of reproducibility in the absolute measurements. Reflectivity data from two unrelated crystals of fully oxygenated ($T_c \simeq 93$ K) $YBa_2Cu_3O_7$ are shown in Fig. 9(a). The dashed lines show the reflectivity at $T \simeq 50$, 100, and 250 K of a crystal (No. 1) studied in June of 1988, which is reproduced from Ref. 31. This crystal was mounted and polished as described above. Also shown in Fig. 9(a) are the reflectivities at $T \simeq 45$, 105, and 250 K for the sample from which the data in the preceding sections was obtained (solid line). This crystal (No. 2) is not polished, and was aligned parallel to its gold reference by careful mounting. Comparing the 50-K and 45-K, the 100-K and 105-K, and the two 250-K curves one can see the high degree of reproducibility obtainable with fully oxygenated $YBa_2Cu_3O_7$ crystals.

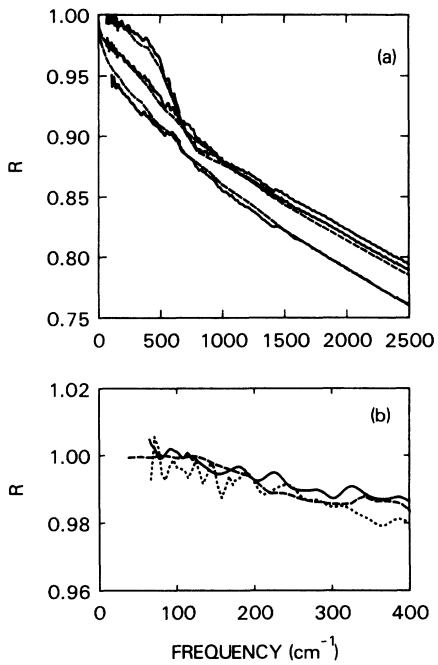

FIG. 9. (a) A comparison of the (a-b)-plane infrared reflectivity of two unrelated fully oxygenated ($T_c = 93$ K) crystals of $YBa_2Cu_3O_7$. Reflectivities at temperatures $T \simeq 50$ K, 100 K, and 250 K are shown. The dashed curves are measurements made on a polished crystal, while the crystal which was used to obtain the solid curves had no surface treatment. (b) A comparison of the low-frequency reflectivities in the superconducting state of a crystal [dotted curve, same data as solid curve at 50 K in (a)], an epitaxial film (solid curve), and the published film data of Schützmann *et al.* (Ref. 95) (dashed curve). All samples were fully oxygenated ($T_c > 90$ K) and were (a-b)-plane oriented. The reproducibility demonstrated in both (a) and (b) is very good ($\sim 0.5\%$).

Because there has been considerable attention recently focused on the issue of very high (100%?) reflectivity at low ω, we examine the reflectivity of both crystals and films at low frequency and temperature in Fig. 9(b). The reflectivities in the superconducting state ($T \lesssim 50$ K) for crystal No. 2, an epitaxial film, and the film data of Schützmann *et al.*[35] are all shown in Fig. 9(b). These data from fully oxygenated crystals and films show very high reflectivity as well as a reasonable level of reproducibility. The film reflectivity data of Karamas *et al.*[76] are lower than these data for $\omega \gtrsim 150$ cm^{-1} for reasons which we do not understand. The question of whether this low-frequency reflectivity reaches 100% at a particular frequency in the far infrared is discussed in Sec. IV B 2.

These results indicate that absolute (a-b)-plane reflectivities are now obtained with acceptable reproducibility for $YBa_2Cu_3O_7$ crystals. This has always been the case with the reflectivity ratios for the fully-oxygenated $YBa_2Cu_3O_7$, which have been quite reproducible from the earliest work[25,28,29,32] to the present.[35,36] In our own

work the earlier problems with absolute measurements were associated with the infrared measurement itself, rather than with substantive intrinsic differences in the crystals.

E. Anisotropy

Using a stack of several $YBa_2Cu_3O_7$ crystals, as described above, we have performed measurements with the infrared electric field polarized perpendicular to the conducting planes.[36] The *c*-axis reflectivities in the normal (100 K) and superconducting (50 K) states are presented in Fig. 10(a). To obtain absolute reflectivities the data was rescaled to account for the open space between individual crystals. (The reflectivity of the epoxy was found to be quite small and was therefore ignored.) Because of these corrections, there is considerably more uncertainty in the absolute reflectivity along the *c* axis than in the (*a*-*b*)-plane data. This uncertainty effects the estimate of how close the low-frequency reflectivity comes to unity in the superconducting state. However, in the normal state the absorption along the *c* axis is large, hence the conductivity is only moderately sensitive to this correction.

The real part of the conductivity, shown in Fig. 10(b), is obtained from a Kramers-Kronig transform of the reflectivity using additional higher-frequency data[77] scaled to match our spectra. The peaks in the normal and superconducting conductivities correspond to *c*-axis polarized phonons at frequencies of approximately 150, 195, 220, 270, 310, and 570 cm^{-1}, while the relatively constant background in $\sigma_{1n}(\omega)$ is presumably electronic. For the *c*-axis direction the electronic contribution to $\sigma_1(\omega)$ is much smaller than for $\mathbf{E}\|a,b$ as expected. Extrapolating the normal-state conductivity to $\omega=0$ as a constant yields an estimate for the *c*-axis dc conductivity of 400 $\Omega^{-1}\,cm^{-1}$, which is about 40 times less than the extrapolated (*a*-*b*)-plane conductivity. This anisotropy (40:1) estimate appears to be at the very low end of the range of values reported from dc transport measurements.

For the *c*-axis direction the electronic and phonon contributions to $\sigma_1(\omega)$ are roughly comparable in magnitude in Fig. 10(b). The phonons are thus not well screened and phonon related features appear prominently in both the reflectivity and in $\epsilon_1(\omega)$ [Fig. 10(c)], which exhibits phonon related zero crossings in this low-frequency region. When the temperature is reduced below T_c we observe an enhancement of the low-frequency reflectivity [Fig. 10(a)], and a corresponding depression of the low-frequency conductivity [Fig. 10(b)] suggesting the opening of a gap in the electronic conductivity. The frequency of the lowest-energy phonon (155 cm^{-1}) increases slightly ($\simeq$2 cm^{-1}) below T_c, while the higher-energy modes exhibit the opposite temperature dependence, decreasing in frequency by from 2 to 5 cm^{-1} near T_c. Some of these phonon-frequency shifts at the transition to superconductivity have been observed in ceramics[17] as well as corresponding changes in the dampings of the phonons,[16] although the present work provides the first identification of the (*c*-axis) polarization of these phonons. One can also observe, in Fig. 10(a), that the

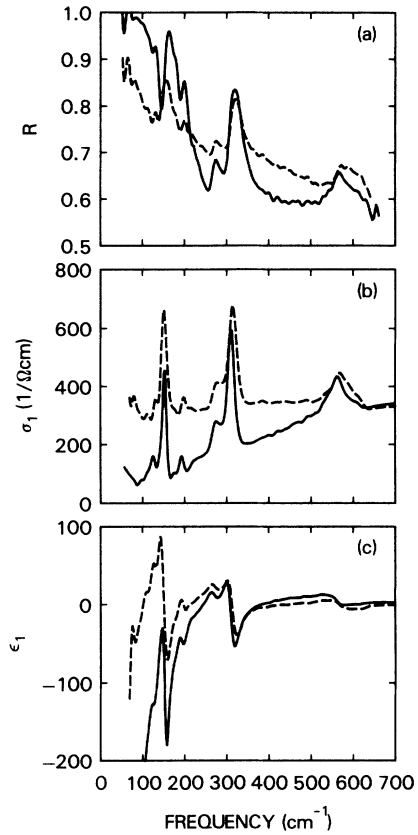

FIG. 10. (a) reflectivity, (b) conductivity, and (c) dielectric response of $YBa_2Cu_3O_7$ with the electric field polarized perpendicular to the CuO_2 planes (i.e., along the *c* axis), are shown for $T=100$ K (dashed curve) and 50 K (solid curve). The relatively constant background conductivity in the normal state [dashed curve of (b)] is electronic, while the peaks in $\sigma_1(\omega)$, and corresponding structures in R and $\epsilon_1(\omega)$, are due to *c*-axis polarized phonons. Note that the electronic conductivity is quite low, hence the relative prominence of the phonons.

reflectivity feature associated with the lowest *c*-axis phonon (155 cm^{-1}) changes from absorptive in the superconducting state to dispersive in the normal state, whereas the higher-frequency phonons always appear dispersively. These observations are consistent with the point of view that the 155-cm^{-1} phonon lies below a gap in the spectrum of electronic excitations, but that the other phonons (at $\omega\geq 195$ cm^{-1}) do not. From this point of view an energy scale of $2\Delta_c\simeq(2-3)kT_c$ could be inferred. This value is consistent with the upper bound that Noh *et al.*[78] have reported for the *c*-axis gap of $La_{2-x}Sr_xCuO_4$, based on studies of the sphere resonance of isolated small particles.

In Fig. 11 the ratio of the reflectivity in the superconducting state (50 K) to that in the normal state (100 K) is shown for both the *c* axis and the *a*-*b* plane, along with the corresponding conductivity ratios. As a consequence of the very low electronic conductivity in the *c* direction, the normal-state reflectivity is quite low and the ratio R_s/R_n tends to be much larger for $\mathbf{E}\|c$ than for $\mathbf{E}\|a,b$. The amplitude of this reflectivity ratio has been reduced

by $\frac{1}{6}$ to allow it to fit on the same scale as the R_s/R_n ratio from the (a-b)-plane measurements. It is quite clear from Fig. 11 that the energy scale associated with the c-axis electrodynamics in the superconducting state is much smaller than for the (a-b)-plane directions; however, the presence of phonons and the corrections discussed above make it difficult to assign a precise value for the c-axis gap (assuming that a true gap exists). Fits of conventional Mattis-Bardeen and Eliashberg forms[36] to the data yield a characteristic energy scale of about 170 cm^{-1}, i.e., $2\Delta_c \simeq 3kT_c$, consistent with the value inferred from the changes in the c-axis phonons, as discussed earlier. More conservatively, one can simply observe, from Fig. 11, that the characteristic energy scale inferred from the infrared data, depends critically on the polarization of the electric field with respect to the principal crystal axes in $YBa_2Cu_3O_7$.

It is interesting to compare the polarized reflectivity ratios in Fig. 11 to the changes in reflectivity which are observed at T_c in ceramic samples of $YBa_2Cu_3O_7$ (see, for instance, Refs. 14 and 15). The strong similarity of the ceramic data to our c-axis ratios appears to confirm the earlier interpretation[22] that ceramic measurements are predominantly sensitive to the c-axis response in the superconducting state. Presumably this results from the large size of the c-axis reflectivity enhancement relative to that associated with the a-b plane. Recent results from $La_{2-x}Sr_xCuO_4$ crystals[39] also provide strong support for this point of view.

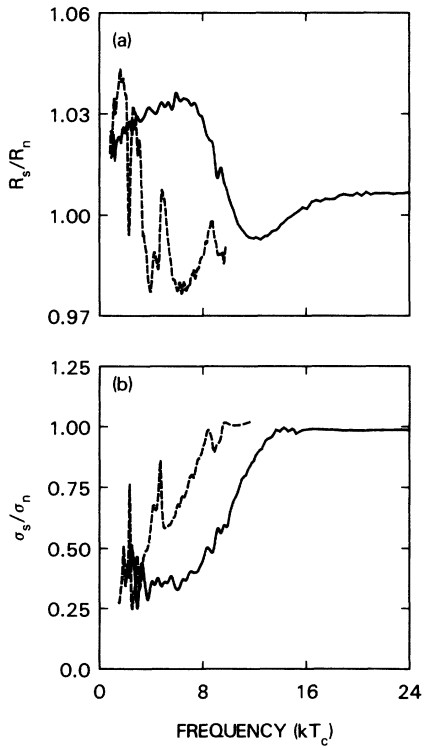

FIG. 11. Superconducting-state anisotropy of $YBa_2Cu_3O_7$. (a) The ratio of the reflectivity in the superconducting state (45 K) to that in the normal state (105 K) is shown for $\mathbf{E}\|a,b$ (solid line) and for $\mathbf{E}\|c$ (dashed line). (b) The corresponding ratios of the real part of the conductivity in the superconducting state to that in the normal are also shown for both polarizations. Considerable anisotropy in the characteristic energy scale associated with the enhancement of the reflectivity and corresponding depression of the conductivity, is clearly evident in the infrared data.

Both the nature and significance of the electronic transport and infrared response associated with the direction perpendicular to the planes is very uncertain. In one view the planes are essentially isolated (transport perpendicular to the planes occurs through Josephson tunneling), and there is only one energy scale in the problem, the (a-b)-plane gap. Reports of extremely short coherence lengths perpendicular to the planes tend to support this approach. If, on the other hand, pairing interactions occur between quasiparticles on different planes, then the concept of distinct energy scales becomes meaningful, and an anisotropic gap with a symmetry no higher than that of the normal state is expected. It has also been suggested that coupling between the planes drives the transition to the superconducting state (in a manner roughly analogous to that in which the coupling between planes in a nearly two-dimensional Heisenberg antiferromagnet is responsible for the transition to long-range order). The number of planes per unit cell is an additional consideration since coupling between planes in the same unit cell may differ fundamentally from coupling between planes in different unit cells. At the present time, the potential theoretical implications of anisotropy in the pair-breaking energy of superconducting $YBa_2Cu_3O_7$ is unclear. In the complex $YBa_2Cu_3O_7$ structure, the smaller c-axis gap could be associated with chains, the presence of which tends to complicate the simple picture of weakly coupled planes given above. Additional polarization-dependent infrared studies of systems with no chains (such as $Bi_2Sr_2CaCu_2O_{8-y}$), or with only one plane per unit cell (for example, $La_{2-x}Sr_xCuO_4$) may be helpful in addressing these issues.

IV. DISCUSSION

A. Normal state

Studies of the normal state of the Cu-O superconductors are based on two complementary motives. First, the question of what Hamiltonian is most appropriate to describe the essential physics of the layered cuprates is best addressed in the normal state (of course, a key test of that Hamiltonian is the nature of its low-temperature ground state). Second, the normal state appears to be interesting in its own right. While it is widely accepted that strong correlation effects are responsible for the insulating behavior of the half-filled band, a key issue which distinguishes the different views of the normal state concerns the manner in which these strong correlations are manifest away from half-filling. Both Hall and infrared measurements are potentially relevant to this question (see, e.g., Refs. 79–81, 33 and 38). In the infrared this issue is closely tied to questions about the total oscillator strength in the free-carrier contribution to the conductivity, and how one models the normal-state conductivity, which is shown in Fig. 3. One fundamental question is

whether the low-frequency conductivity should be associated with $(1-\delta)$ electrons per Cu site, which is the prediction of Fermi-liquid theory[82], or δ holes per Cu site, as predicted in RVB and other highly correlated approaches to the normal state.[83] (Here δ is the deviation from half-filling per Cu site.) This issue can become quite subtle when mass enhancement, which can depend strongly on filling (δ), is included. Another fundamental question is the degree to which the infrared conductivity reflects the presence of low-energy charge or spin excitations, which may be directly or indirectly relevant to the superconducting mechanism. These issues are considered in the following discussion.

1. *Infrared sum rules*

In Fig. 12 the integrated normal state (a-b)-plane conductivity at 100 K is shown for fully-oxygenated ($T_c \simeq 93$ K) $YBa_2Cu_3O_7$ and for an oxygen-deficient film sample with $T_c \simeq 60$ K. The units used are carriers per unit cell, $n(\omega)$, where

$$n(\omega)=\frac{2m_b}{\pi}\int_0^{\omega}\sigma(\omega')d\omega' . \quad (1)$$

Note that the relevant mass m_b is the high-frequency optical mass, rather than the (enhanceable) low-frequency mass. In Fig. 12 we have arbitrarily chosen m_b to be the free-electron mass. [In our notation $n(\omega)$ may be either an electron or hole density depending upon which of the above views of the normal state is most meaningful.] For fully oxygenated $YBa_2Cu_3O_7$ ($T_c=93$ K), the area contained in $\sigma_1(\omega)$ up to 10 000 cm^{-1} corresponds to roughly one hole per unit cell ($\omega_p \simeq 23\,000$ cm^{-1}), which is the value predicted by naive formal valence arguments. For the $YBa_2Cu_3O_{7-x}$ $T_c \simeq 60$ K film (nominally $x=0.4$), we get an area corresponding to about 0.5 holes per unit cell with the same (10 000 cm^{-1}) high-frequency cutoff.

Attempting to analyze the variation of $n(\omega)$ with x in $YBa_2Cu_3O_{7-x}$ is a formidable task with both theoretical and experimental uncertainties. The choice of optical mass is rather arbitrary, as is the high-frequency limit of integration, since there is no clear separation of the low-frequency conductivity from the large interband contributions at higher frequency. Variation of the oxygen content changes the coordination of the chain Cu, and presumably its valency as well, introducing further complexity (and disorder). As a consequence there is no Hubbard insulator at $x=0.5$ to which deviations from a half-filled band could be reliably referred. (Pr or Nd doping at the Y site might provide a more controlled way in which to vary δ.) Even at $x=0$ (i.e., O_7), there is ambiguity associated with the distribution of holes between the chains and planes. Theoretical considerations originating from the point of view of a lightly-doped Hubbard insulator place all the holes on the planes, however, Tokura *et al.*[81] have argued that the holes are divided between the chains and planes with 0.5 holes per chain Cu and 0.25 holes per plane Cu (for a total of one hole per unit cell) in $YBa_2Cu_3O_7$. Very recent polarized infrared data[37] seem to be consistent with a very large fraction of holes on the chains (~ 0.6 per Cu), and ~ 0.2 holes per plane Cu (close to the value of δ where $La_{2-x}Sr_xCuO_4$ exhibits maximum T_c), although data extending to higher frequencies may be required to make this interpretation completely unambiguous.

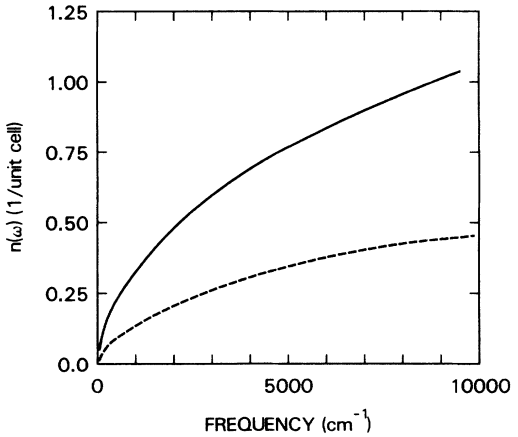

FIG. 12. Effective carrier density as a function of frequency, ω, for a $T_c=93$ K crystal (solid line) and an oxygen-deficient film ($T_c \simeq 60$ K) (dashed line) are shown. The solid line is obtained from the integrated area of the 105 K conductivity in Fig. 3(b), and is expressed in units of carriers per unit cell, where $m_b=m_e$ has been assumed.

2. *Temperature dependence of the infrared and dc conductivities*

In Fig. 4(b), the conductivity exhibits a peak at low frequency. The growth of this peak as temperature is reduced is suggestive of the normal-state temperature dependence of σ_{dc}. the actual infrared data extend down to about 70 cm^{-1}, which is too high a frequency to permit a direct comparison between the infrared and dc conductivities, since the width of the peak is only about 150 cm^{-1} at 100 K. To make a quantitative comparison, a procedure for extrapolating to lower frequency is required. For technical reasons it is very difficult to extrapolate the conductivity directly and still satisfy the constraints placed on $\sigma_1(\omega)$ by the Kramers-Kronig relations. As described in Sec. II, we have instead attached a Hagen-Rubens form to the reflectivity data at low frequency, and transformed the resulting spectrum to obtain $\sigma_1(\omega)$ down to $\omega=0$. Extrapolated estimates for the dc resistivity as a function of temperature obtained in this way are shown in the inset to Fig. 4(b). These values are reasonably consistent with typical measured dc resistivities both in terms of their approximately linear temperature dependence and their overall magnitude, suggesting that our extrapolation to $\omega=0$ is not unreasonable. [Note, however, that it has not been directly shown that the low-frequency dynamics are Drude-like, and other novel forms of $\sigma(\omega)$ are possible.]

As discussed earlier, there is a sum rule on the total conductivity, thus the increase in $\sigma_{1n}(\omega)$ at low frequency in the normal state must be accompanied by a corresponding decrease at higher frequency. In Fig. 4(b) one observes that the conductivity at 105 K is considerably

higher than that at 250 K, for $\omega \lesssim 300$ cm^{-1}, and slightly lower in the range $300 \lesssim \omega \lesssim 600$ cm^{-1}. Because the excess area in the conductivity at 105 K exceeds the deficit in this restricted frequency range, this data suggests that conductivity changes extending to higher frequency are also occurring. The relevant question is, up to what frequency must we integrate $\sigma_1(\omega)$ so that the integral will be independent of temperature? This question is difficult to address directly because cumulative errors develop in integrating $\sigma_1(\omega)$, which are comparable to the small changes we are attempting to study. [The cumulative error has both numerical origins (noise related), and systematic origins associated with the fact that $\sigma_1(\omega)$ is obtained via a Kramers-Kronig transform.] A more robust way to consider the sum rule question is through a direct examination of the reflectivity. If the sum rule were satisfied within a fairly modest frequency range (e.g., of order several kT), then the reflectivity would not be significantly temperature dependent above that frequency range. The observation that the reflectivity is almost uniformly temperature dependent up to ~ 8000 cm^{-1}, indicates that one must integrate up to a frequency of that magnitude to satisfy the sum rule. In other words, the conductivity that is going into the temperature-dependent peak near $\omega=0$, appears to be coming from a very broad range of frequencies in the infrared, as previously reported.[31] Qualitatively, this behavior is typical of a frequency-dependent scattering model,[31] although the proper way to model the normal-state dynamics remains open, as discussed Sec. IV A 3.

3. *Modeling the normal-state data*

The normal state (a-b)-plane conductivity of $YBa_2Cu_3O_7$ has been previously interpreted in terms of two conceptually different models. Both models are attempts to deal with the observation that the infrared conductivity does not diminish with frequency as rapidly as one expects for a simple weak-coupling Drude picture [i.e., $\sigma_1(\omega) \propto 1/\omega^2$]. Instead there is a very broad background conductivity, which persists throughout the infrared as seen in Fig. 3(a). Both models also implicitly assume that this background conductivity is associated with the CuO_2 planes. It is also possible that some of this background conductivity may not be intrinsic to the planes, but may instead be associated with the presence of chains or extrinsic loss mechanisms. To study the normal-state dynamics in the infrared, one measures reflectivity (over a wide frequency range), and Kramers-Kronig transforms that data to obtain conductivity as a function of ω. One approach to the cuprate data has been to divide the conductivity into two parts, one associated with a mid-infrared mode and the other with the free carriers.[29] Another has been to describe the low-frequency dynamics in terms of a strongly frequency-dependent scattering rate.[30,31] These two formulations are not mutually exclusive. The division of $\sigma(\omega)$ into two parts is certainly necessary above 1.5 eV, and may be relevant near ~ 1 or ~ 0.5 eV (4000 cm^{-1}). At the same time the scattering rate for the Drude term must have a frequency dependence at lower ω corresponding to the T dependence of ρ_{ds}.

(a) *Spin-interaction picture.* In one version of the frequency-dependent scattering approach, essentially all of the conductivity below about 8000 cm^{-1} (~ 1.5 eV) is accounted for within a single strongly coupled band. An interaction between the charge carriers and a spin-related excitation spectrum causes both the carrier mass and scattering rate to be strongly frequency (and temperature) dependent. In this picture, mass enhancement at low frequency is associated with a "spin-excitation cloud" which is dragged along by the carrier, while at high frequency (i.e., $\omega \gtrsim$ the characteristic spin-excitation frequency) the carrier motion becomes too rapid for the spin excitations to follow, and thus the carriers shed their mass enhancement. The scattering rate increases correspondingly from a relatively low value at low ω, to a much higher one at high ω as the inelastic scattering process become energetically allowed. The conductivity that results from such strong inelastic scattering exhibits a coherent peak at low frequencies, and a broad incoherent background extending to much higher frequency. Roughly speaking, the total area in the conductivity (coherent plus incoherent), divided by the area of the coherent peak alone, provides an approximate measure of the mass enhancement ($m^*/m_b = 1+\lambda$) and, hence the coupling strength (λ). Based on this approach, coupling strengths of $\lambda \simeq 10$ and $\lambda \simeq 3$ were originally reported for $YBa_2Cu_3O_{7-x}$ ($x \simeq 0.3$, $T_c \simeq 50$–70 K) and $YBa_2Cu_3O_7$ ($T_c \simeq 92$ K), respectively.[30,31] As discussed later the former value appears to have been overestimated; roughly similar values (near $\lambda=3$) are now obtained for both the fully oxygenated ($T_c=92$ K) and $T_c \simeq (50$–$60)$-K samples with this approach.

In a phenomenological approach similar to that pioneered by Sievers and co-workers[84–86] (to treat mass enhancement in heavy-Fermion and mixed-valence compounds), one can express the conductivity in terms of a frequency-dependent mass and scattering rate as[31]

$$\sigma(\omega)=\frac{ne^2\tau^*(\omega)}{m^*(\omega)[1-i\omega\tau^*(\omega)]} . \tag{2}$$

Here $m^*(\omega)=m_b[1+\lambda(\omega)]$ is the renormalized mass and $1/\tau^*(\omega)=1/\tau(\omega)[1+\lambda(\omega)]$ is the renormalized scattering rate. In this generalized Drude form (also referred to as memory function formalism), the unrenormalized scattering rate, $\tau^{-1}(\omega)$ and the coupling $\lambda(\omega)$ are related by causality through a Kramers-Kronig relation.

Using the measured conductivity (real and imaginary parts) one can calculate the scattering rate and mass at each frequency with Eq. (2). In this calculation we use $n/m_b = 6\times 10^{21}$ cm$^{-3}/m_e$ (which corresponds to about 1 hole per unit cell), based on the conductivity sums discussed earlier. The value of n/m_b sets the plasma frequency ($\omega_p^2 \propto n/m_b$) and is proportional to the total area in the free-carrier contribution to the conductivity. In Fig. 13 we show $\tau^{-1}(\omega)$ and $m^*/m_b = 1+\lambda(\omega)$ as a function of frequency for $YBa_2Cu_3O_7$ at 100 K as calculated from Eq. (2). The frequency dependence of τ^{-1} is most rapid below about 1000 cm^{-1} which roughly sets the frequency scale for the inelastic scattering spectrum. The

low-frequency value of $\lambda(\omega)$ indicates an overall coupling strength of $\lambda \simeq 3$, in agreement with the above estimate based on conductivity sum rules. A more detailed attempt to model the data from a spectral density $\alpha^2F(\omega)$ is discussed in Ref. 31.

Note that the coupling obtained from Eq. (2) is quite sensitive to the value of n/m_b used, and thus will be inaccurate if there are contributions to $\sigma(\omega)$ in the frequency range of interest, that are not intrinsic to the CuO_2 planes. If part of the conductivity below 10 000 cm^{-1} is associated with interband or chain contributions, then the actual value of the coupling would be less than the value shown in Fig. 13. For example, subtracting a chain contribution consistent with Ref. 37 from the total conductivity, one obtains $n/m_b \simeq 3\times10^{21}$ cm^{-3}. Using this value is Eq. (2), one then obtains a revised estimate for the low-frequency mass enhancement of about 2. The frequency content of the excitation spectrum to which the carriers couple is not dramatically changed. The scattering rate and mass enhancement as a function of frequency for this case are shown in Fig. 13 (dotted curves). This smaller coupling may in fact be more nearly representative of the intrinsic nature of the CuO_2 planes. Initial work on $Bi_2Sr_2CaCu_2O_{8-y}$,[87] which has no chains, is also interpretable in terms of a similarly modest value of λ.

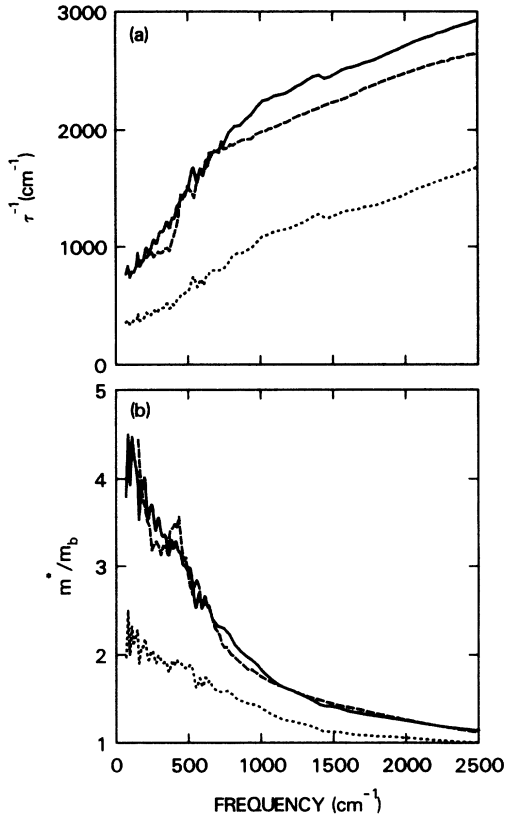

FIG. 13. (a) Frequency-dependent scattering rate and (b) mass enhancement derived from the (*a-b*)-plane conductivity data as described in the text, are shown for a $T_c \simeq 93$-K (solid curve), and a $T_c \simeq 60$-K (dashed curve) $YBa_2Cu_3O_{7-x}$ film. The dotted curve shows the effect of subtracting off a chain contribution to the conductivity (based on Ref. 37) before performing the frequency-dependent scattering analysis. An overall coupling strength of $\lambda \simeq 1$ to 3 to a broad spectrum extending up to about 1000 cm^{-1} (nJ) is inferred from this approach to the infrared data.

In the earlier work of Sulewski *et al.*[21] and Thomas *et al.*,[30] similar approaches were applied to polycrystalline and reduced-T_c $YBa_2Cu_3O_{7-x}$ samples, respectively. In the latter case the coupling spectrum was very similar to that which we find for fully oxygenated $YBa_2Cu_3O_7$, but a substantially larger mass enhancement, $\lambda \simeq 10$, was originally reported in Ref. 30. In that work a plasma frequency of $\simeq 24\,000$ cm^{-1}, i.e., $n/m_b = 6.0\times10^{21}$ cm^{-3}/m_e, was used, which is about the same value we have used for our 93-K material. Since the area in the low-frequency (coherent) peak is much smaller in the oxygen-deficient samples, this leads to the much larger estimate for the coupling in their work. In our own work on oxygen-deficient samples with T_c near 60 K, using the same limit of integration as for the 93-K material, we obtain lower values of n/m_b, and estimates for λ between about 3 and 5. In Fig. 13 we include $\tau^{-1}(\omega)$ and $\lambda(\omega)$ for the $T_c = 60$-K film sample for which conductivity sums were given in Fig. 12. The inclusion of conductivity from higher frequencies in estimating n/m_b could account for the higher estimate for λ in the original work on oxygen-reduced $YBa_2Cu_3O_{7-x}$.[30]

In the strong-coupling approach to the conductivity discussed earlier, the characteristic frequency scale ($\omega \lesssim 1000$ cm^{-1}) associated with the mass enhancement is considerably higher than that for the heavy-Fermion compounds ($\omega < 50$ cm^{-1}), while the magnitude of the coupling is much lower. This approach is presumed to describe an interaction between holes (or holons) and spin-related excitations (or spinons) associated with the Cu. Within this context one may consider various non-Fermi-liquid approaches,[83,88–90] as well as more conventional heavy-Fermion approaches.[84–86] A detailed calculation of the quasiparticle residue in a *t-J* model with Neel or an RVB order[90] shows a low-frequency mass enhancement of t/J, which occurs below a characteristic energy J, where J is the antiferromagnetic exchange energy. Values of t/J of order 1–3 are not at all unreasonable,[91] however, they place the models in an intermediate range where calculations tend to be quite difficult. Although the formalism we have used here [Eq. (2)] is similar to that used for the heavy fermions, the result for the scattering rate appears to be fundamentally different. In particular, as we have reported previously, "the inelastic contribution to $\hbar/\tau^*$ is of order $kT+\hbar\omega$, suggesting a nearly localized Fermi liquid or that $Y_1Ba_2Cu_3O_7$ is at the edge of the regime in which a Fermi-liquid theory is well defined."[31] This linearity of $1/\tau^*$ in the frequency domain has a direct correspondence with the linearity of ρ versus T, and provides an early example of *apparently non-Fermi-liquid behavior* in the normal state of a cuprate superconductor.

(b) *Charge excitation picture.* As an alternative to the above approach, one can divide the normal-state conductivity into two distinct components: a narrow Drude (or free-carrier) peak at low frequency, which may be modified to allow for weak coupling to phonons ($\lambda \lesssim 0.5$), and a broad mid-infrared contribution or "mode". In

this weak-coupling approach the "mid-infrared conductivity" is defined to be the difference between a calculated "ordinary" free-carrier conductivity and the measured spectrum. In $YBa_2Cu_3O_7$ the conductivity decreases monotonically from $\omega=0$ up to above 10 000 cm^{-1}, thus the term mid-infrared "mode" may be misleading. Phenomenologically, the strong- and weak-coupling pictures are opposite endpoints on a continuous spectrum of models in which the coupling becomes progressively weaker as more and more of the infrared conductivity is ascribed to sources other than a single free-carrier band.

A specific example of a decomposition of the $YBa_2Cu_3O_7$ (a-b)-plane conductivity into a free-carrier component and a background conductivity is shown in Fig. 14. The free-carrier conductivity is calculated from the Eliashberg equations as discussed by Bickers *et al.*,[92] with a carrier density of $n=2.0\times10^2$ cm^{-2}, a renormalized elastic scattering rate of 150 cm^{-1} and a coupling of $\lambda=0.5$ to a (phonon) spectrum extending up to 500 cm^{-1}. The background conductivity is obtained by subtracting this free-carrier term from the measured conductivity. In the frequency range below 10 000 cm^{-1} about $\frac{2}{3}$ of the conductivity is in this slowly varying background contribution, and about $\frac{1}{3}$ of the conductivity is in the free-carrier contribution. While this approach classifies the conductivity, it does not explain its origin. To do so one must attribute the background conductivity to a specific physical process, one proposal for which is a severly broadened charge-transfer excitation (of holes) from oxygen to copper. In this picture the conductivity reflects the presence of a low-lying charge excitation in the planes.

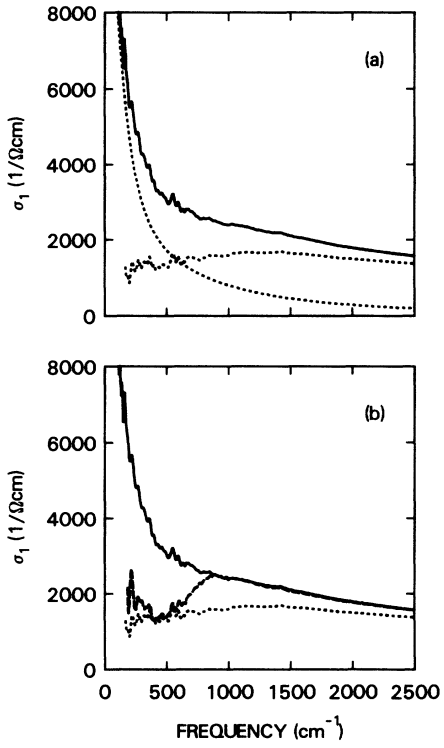

FIG. 14. (a) Deconstruction of the measured normal-state conductivity at 105 K (solid line) into a weakly coupled ($\lambda\simeq0.5$) free-carrier part, peaked at $\omega=0$, and a background conductivity (dotted lines), which is the difference between the measured conductivity and the calculated free-carrier term, is shown. In (b) the measured normal- (solid line) and superconducting-state (dashed line) conductivities are shown along with the background conductivity from (a) (dotted line). Note that this background conductivity looks different from $\sigma_{1s}(\omega)$ in that it approaches $\sigma_{1n}(\omega)$ very gradually at high frequency.

As mentioned earlier, the presence of conductivity in the mid-infrared is closely related to the absence of a pronounced reflectivity minimum and the broadened nature of the plasma edge in the reflectivity. Electronic inhomogeneity, especially in the carrier density, can also contribute to the width of the plasma edge [i.e., the abruptness with which the reflectivity drops in the vicinity of the zero crossing of $\epsilon_1(\omega)$]. It has not been shown experimentally that this is a negligible effect, although for the fully oxygenated $YBa_2Cu_3O_7$ one expects a high degree of homogeneity. It is possible that a significant fraction of the mid-infrared conductivity in $YBa_2Cu_3O_7$ is chain related, as mentioned earlier.

B. Superconducting state

In this section we examine the very unusual properties of $YBa_2Cu_3O_7$ in the superconducting state. We discuss the gaplike feature in $\sigma_1(\omega)$ at 500 cm^{-1} ($\simeq8kT_c$) which appears near T_c, and show that the area missing from the conductivity due to this gap gives an accurate estimate of the low-temperature penetration depth. Unconventional aspects, including the temperature dependence, the large energy gap ($2\Delta_{a\text{-}b}\simeq8kT_c$), and possible evidence for fluctuation effects above T_c are discussed. The possibility of a second gap in the infrared spectra with a smaller, more conventional magnitude is also considered. We find no clear evidence for such a feature in either the (a-b)-plane reflectivity or conductivity. Experiments with the electric field polarized perpendicular to the planes do show evidence for a lower energy scale ($\sim3kT_c$) in the superconducting state. Finally, we compare the $YBa_2Cu_3O_7$ reflectivity with similar data from the cubic oxide superconductor $Ba_{1-x}K_xBiO_3$ ($T_c\simeq30$ K).[70] Qualitatively, the infrared behavior of these two superconductors is strikingly similar. Applying the same analysis to both sets of data yields a conventional energy scale, $2\Delta_c\simeq4kT_c$, for $Ba_{1-x}K_xBiO_3$, and the highly unconventional result $2\Delta_{a\text{-}b}\simeq8kT_c$ for the (a-b)-plane response of $YBa_2Cu_3O_7$.

1. *The characteristic energy* $2\Delta_{a\text{-}b}\simeq8kT_c$

In the (a-b)-plane data from $YBa_2Cu_3O_7$, the enhancement of the low-frequency reflectivity for $T<T_c$ [Fig. 5(a)] leads to a reflectivity ratio, R_s/R_n, which is peaked at $\simeq500$ cm^{-1} (Fig. 1). In both the absolute conductivity shown in Figs. 5 and 6, and the conductivity ratios σ_s/σ_n in Fig. 8, there is a corresponding threshold at approximately 500 cm^{-1} above which the superconducting conductivity rises rapidly back to the normal-state value. From these observations we identify a characteristic energy scale of about 500 cm^{-1} ($\simeq60$ meV, $\simeq700$ K, $\simeq8kT_c$)

for this gaplike feature. The detailed temperature dependence shown in Figs. 6 and 7 clearly associates this feature with the superconducting state.

A simple way in which to view $\sigma_{1s}(\omega)$ is as the superposition of a free-carrier conductivity spectrum with a gap at 500 cm^{-1}, and a roughly constant background conductivity at a level of about 1200 $\Omega^{-1}cm^{-1}$. The reproducibility of the data suggests that much of this background conductivity is intrinsic to the bulk material, however, the possibility of some extrinsic absorption due to impurity phases or imperfections near the surface can never be completely ruled out. Assuming that this background conductivity is intrinsic, *one possible source is the b-axis chains in* $YBa_2Cu_3O_7$, which may contribute to the infrared conductivity if there are mobile, or not too strongly localized holes, on the chains. A recent polarized measurement of an untwinned crystal has reported a chain conductivity which is roughly constant at about 1300 $\Omega^{-1}cm^{-1}$ for $\omega \lesssim 2000$ cm^{-1}.[37] This is potentially sufficient to account for the finite value of $\sigma_{1s}(\omega)$ below the 500 cm^{-1} gap. The question of how such a chain contribution would appear in a twinned crystal has not been worked out in detail, although presumably some sort of averaging (possibly utilizing an effective medium theory) should provide a reasonable approximation. As discussed in detail later, it is very difficult to tell from the infrared measurement if there is, in fact, an additional gap at a lower frequency in this background conductivity. Within the present context this would correspond to a smaller gap on the chains [which may be suggested by some nuclear quadrupole resonance (NQR) experiments[64,69]].

Another possible source of finite absorptivity below 500 cm^{-1} is an anisotropy of the energy gap in k space, as suggested by the c-axis measurements (Sec. III E). While it is conceptually convenient to assume that measurements made with the electric field parallel to the planes are only sensitive to those points in k space which lie within the plane, this is only true when the penetration depth is much shorter than the mean-free path.[93] In the a-b plane of $YBa_2Cu_3O_7$ the penetration depth is large, hence the dynamics are closer to the local limit in which scattering will mix, to some extent, contributions from all directions in k space into the $(a$-$b)$-plane response. In this case, the conductivity should be strictly zero only below the smallest gap in the system (possibly the c-axis gap, as discussed in Sec. III E). It is difficult to estimate the extent of this mixing in such a complex and poorly understood system as $YBa_2Cu_3O_7$. Schneider[94] has discussed this point on the basis of a specific model for a highly anisotropic superconductor.

As discussed in Sec. III B and in Sec. IV B 2 there is too much uncertainty in $\sigma_{1s}(\omega)$ at low frequency to determine whether the conductivity actually becomes identically zero below some finite frequency. In principle, this seems to leave open the possibility of an unconventional pairing symmetry with modes in the (a-b)-plane gap, (e.g., d-wave pairing), however, the abruptness of the threshold in $\sigma_{1s}(\omega)$ at $\simeq 500$ cm^{-1} (Figs. 6 and 8), and of the drop in R_s/R_n (Fig. 1), are both highly suggestive of an s-wave gap. Additionally, the lack of temperature dependence in the infrared data for $T < 50$ K seems inconsistent with the existence of excitations to arbitrarily low energy. This lack of temperature dependence in the infrared data is consistent with the reported temperature independence of the penetration depth[45,46] in the same range, which has also been interpreted as evidence for s-wave pairing symmetry. In view of these results, it seems highly unlikely that the finite conductivity below 500 cm^{-1} is associated with a pairing function with nodes in the a-b plane.

2. *Possible evidence for a BCS gap* ($2\Delta \simeq 3.5kT_c$)

An interpretation of infrared data from oxygen-deficient crystals in terms of an energy gap of conventional magnitude ($2\Delta \simeq 3.5kT_c$), based on the criterion of 100% absolute reflectivity has been proposed by Thomas *et al.*[30] In this section we examine both the question of determining a frequency at which the absolute reflectivity reaches 100%, and the possible evidence for a BCS size gap in the infrared data.

In Fig. 9(b) we have shown the reflectivities in the superconducting state for crystal No. 1,[36] our epitaxial film, and the film data of Schutzman *et al.*[35] These measurements all probe the $(a$-$b)$-plane response of fully oxygenated ($T_c \gtrsim 90$ K) $YBa_2Cu_3O_7$, and show that very similar results are obtained with crystals and films, even in different laboratories. Below $\omega \lesssim 150$ cm^{-1} these data show a reflectivity between about 99.5% and 100.5%. From the data we are unable to extract a particular frequency at which the reflectivity becomes equal to 1, although the results could be viewed as consistent with a reflectivity of unity, within experimental error, up to any frequency less than 150 cm^{-1}. The question of whether R actually reaches unity at some finite frequency is very significant conceptually, but clearly very different to address experimentally. The data of Shutzman *et al.*[35] is the least noisy, and therefore best suited to address this question. (Actually, the wiggles in the data are primarily due to interference effects which tend to be prominent at low ω and very difficult to control, rather than due to noise which can be averaged away. These effects are relatively large in our data and that of Thomas *et al.*[30] however, Shutzman *et al.*[35] have developed methods to minimize these effects and thus obtain improved low-frequency data.) Although earlier reports based on the spectrum we have reproduced in Fig. 9(b) suggested unit reflectivity below about $2kT_c$,[35] more recent data from Shutzman, Renk *et al.*[95] indicate that the reflectivity increases continuously toward unity throughout the infrared with no clear frequency at which R becomes 100%. Our own results also appear to be in agreement with the later interpretation.

This discussion illustrates how difficult it is to resolve issues centered on the existence of perfect reflectivity at low frequency. [Problems associated with establishing a region in which $\sigma_{1s}(\omega)=0$ at low ω are even more severe, as discussed in Sec. III B.] In any event, we are unable to find evidence for a $3.5kT_c$ energy scale in either the absolute reflectivities or the reflectivity ratios for the a-b plane of $YBa_2Cu_3O_7$.

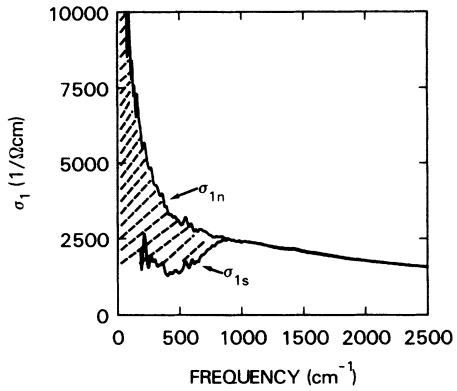

FIG. 15. (a) The (a-b)-plane conductivity of $YBa_2Cu_3O_7$ in the normal state (105 K) and superconducting state (45 K) are shown. The missing area in the superconducting state, shown by the shaded region, provides an estimate for the (a-b)-plane penetration depth of $c/\sqrt{8A}=1700$ Å.

3. *The penetration depth and the infrared conductivity*

On quite general grounds, one expects that the area that is missing from the conductivity due to the formation of the superconducting gap (Fig. 15) will appear in a δ function at $\omega=0$. The δ function, rather than the gap itself, is the truly unique and essential feature of the superconducting state. The area in this δ function (A) controls the low-frequency electromagnetic penetration depth, thus the validity of our infrared data can be tested by using it to calculate the penetration depth at low temperature. In terms of the infrared conductivity the penetration depth is given by,

$$\lambda=c/\sqrt{8A}\ , \tag{3}$$

where

$$A=\int(\sigma_{1n}-\sigma_{1s})d\omega\ . \tag{4}$$

In the clean limit ($l/\xi=\infty$) all of the free-carrier conductivity collapses into the δ function, in which case $A=\pi e^2 n/2m_b=\omega_p^2/8$, and Eq. (3) reduces to the familiar London result, $\lambda=c/\omega_p$. For finite l/ξ the penetration depth tends to be larger than this limiting value and one can write $A=\pi e^2 n_s/2m_b$, where $n_s<n$ is the superfluid density. In general, one can calculate A, and hence λ, from the data without making any assumptions about cleanliness or even the specific model of the superconducting state. To calculate A in this general way we use $\sigma_{1s}(\omega)$ at 45 K, and the conductivity at $T=105$ K for $\sigma_{1n}(\omega)$. Below 150 cm^{-1} we extrapolate $\sigma_{1s}(\omega)$ to $\omega=0$ as a constant, however, this extrapolation [compared to setting $\sigma_{1s}(\omega)=0$ below 150 cm^{-1}] makes less than 10% difference to the penetration depth calculation since the area under $\sigma_{1s}(\omega)$ at low ω is quite small in any case. The primary source of uncertainty in our infrared estimate of λ is actually associated with the value of $\sigma_{1n}(\omega)$ below $\sim$100 cm^{-1}, which is obtained from our low-frequency extrapolation, as discussed in Sec. IV A. Underestimating the normal-state conductivity in this region would cause us to overestimate λ, however, because of the square root in Eq. (3) the final result is not particularly sensitive even to this extrapolation. Integrating the infrared conductivities, we obtain $\lambda\simeq1700$ Å (which formally corresponds to a superfluid density, n_s, of about 1×10^{21} cm^{-3} if one assumes $m_b=m_e$). This value of λ obtained from the infrared data is comparable to values of the penetration depth obtained by μsr,[46] as well as direct magnetic measurements,[45] which are typically about 1500 Å for the a-b plane of $YBa_2Cu_3O_7$. This agreement indicates that the conductivity that is "missing" from $\sigma_{1s}(\omega)$ up to $\omega\simeq800$ cm^{-1} is indeed the conductivity that goes into the δ function at $\omega=0$ in the superconducting state.

In the same manner, the c-axis conductivities in Fig. 10(b) can be used to estimate the strength of the δ function for the out-of-plane direction. For the c axis, a result corresponding to the formal value $\lambda\simeq1$ μm is thus obtained.

4. *Temperature dependence and fluctuation effects*

Although Figs. 5–7 clearly demonstrate that the $8kT_c$ feature in the a-b plane is associated with the superconducting state, several aspects of this temperature dependence are unusual and warrant further consideration. In Fig. 6, the amplitude of the conductivity at low frequency drops rapidly below T_c, but it seems that the characteristic energy scale over which the conductivity is depressed is rather insensitive to temperature, as illustrated in Fig. 8(b). For example, the depression of the conductivity at 80 K has virtually the same energy range ($\omega\lesssim500$ cm^{-1}) as seen deep in the superconducting state. This is also apparent in the reflectivity ratios (R_s/R_n) in Fig. 7, in which the frequency of the minimum in R_s/R_n remains nearly constant as T approaches T_c. This data strongly suggests an order parameter which opens much more rapidly below T_c than in mean-field theory. Other evidence for this point of view can be found in the specific-heat jump which is narrower and drops much more rapidly below T_c than mean-field theory would predict.[42–44] Rapid development of the real part of the energy gap may also be tied to the absence of an Hebel-Slichter peak below T_c in NQR (Refs. 63–69) and microwave absorption measurements (Refs. 96 and 97).

The size of our (a-b)-plane pair breaking energy ($8kT_c$) is roughly twice the BCS prediction ($3.5kT_c$). Given this observation, rapid development of order below T_c does not seem unreasonable. In principle, extremely strong coupling could account for an unusually large reduced gap, but, as discussed in Sec. IV B 5 strong modification of the density of states above 2Δ (which should be easily observed if such strong coupling occurs) is not apparent in our data. Short-range-order and fluctuation effects can also suppress T_c relative to mean field, particularly in systems with an extremely short coherence length or lower dimensionality. If short-range order begins to grow well above T_c, the local order parameter (which is at least in part responsible for setting the energy scale we see in the infrared) could already be well developed at T_c even in the absence of long-range order. Evidence for superconducting fluctuations extending to temperatures as high as $2T_c$ has been reported in resistivity,[98–100] specific-heat,[101]

and susceptibility[102] studies of $YBa_2Cu_3O_7$. However, in most cases these fluctuations have been discussed within the Aslamazov-Larkin formulation and its variations, which are based on fluctuations about mean-field behavior and are not expected to provide an appropriate description of the large-scale-fluctuation effects which would be necessary to strongly suppress T_c. As noted in Sec. II, the conductivity ratios in Fig. 8 may also provide some evidence for fluctuation effects above T_c. In the 105-K ratio there is a small minimum near 500 cm^{-1} that is reminiscent of the large gap which develops in the superconducting state. This could be taken as evidence for local order at temperatures above T_c, however, it is somewhat difficult to distinguish this feature from the temperature dependence that occurs in the normal state, associated with the linear resistivity and consequent narrowing of the conductivity peak. This difficulty is due to the fact that characteristic frequencies of the normal and superconducting state changes are very similar ($\simeq 500$ cm^{-1}). One can speculate that this similarity of energy scales is not merely a coincidence, but rather a fundamental feature of the layered copper-oxide superconductors.

5. *Possible Holtstein interpretation*

As shown by the temperature dependence in Figs. 6 and 7, the phenomenology of the 500-cm^{-1} feature is intimately connected with the transition to superconductivity is fully oxygenated $YBa_2Cu_3O_7$. Because of this correlation with superconductivity, it is natural to associate this absorption threshold with some sort of pair-breaking excitation with a characteristic energy of 500 cm^{-1}. In principle, another possibility is that the 500-cm^{-1} feature is associated with a higher-order process, involving the simultaneous breaking of a superconducting pair and emission of an intermediate excitation. In a conventional superconductor this is referred to as a Holtstein process and the emitted boson is a phonon.[6-8] In this section we consider the possibility that the 500-cm^{-1} feature which is prominent in the infrared data could be associated with such a Holstein process. To investigate this possibility we have used a generalized Eliashberg theory, allowing for finite mean-free path and coherence length.[92] The Eliashberg equations are solved at the Matsubara points along an imaginary frequency axis, and continued to the real axis by Pade approximates to obtain $\sigma(\omega)$. Inputs to the calculation include carrier density, elastic scattering rate, temperature, and the fluctuation spectrum, $\alpha^2F(\omega)$. Describing the 500-cm^{-1} feature as a Holstein effect requires a fluctuation spectrum peaked at about 300 cm^{-1} with a total coupling strength of $\lambda \simeq 1.5$. This coupling spectrum implies a T_c of about 80 K, thus this interpretation of the infrared data would lead to a fairly complete phenomenology of the superconducting mechanism. One of the problems with this approach is that it predicts a superconducting gap at about 200 cm^{-1} which is not seen in the data. In addition, the fit to the infrared data between 400 and 1400 cm^{-1} is not very good despite the wide range of parameters available, and the temperature dependencies implied by this model in both the normal and superconducting state for $\sigma(\omega)$ and σ_{dc} are also not easily reconciled with measured values. These problems suggest that describing the 500-cm^{-1} feature as a Holstein step is not a meaningful way in which to view the infrared data.

The association of the 500-cm^{-1} feature with an elementary pair excitation seems to be more consistent with the data. Within this context one can consider the question of whether there are Holstein-like structures above this 500-cm^{-1} gap. Using the Eliashberg equations, again as formulated by Bickers *et al.*,[92] this approach does not lead to a self-consistent solution with $T_c \leq 100$ K. If we do not constrain T_c, then a class of solutions consistent with the infrared data can be found. In these solutions, weak coupling to a high-frequency excitation is used as a formal device to generate the large gap. This, in turn, leads to $T_c \simeq 200$ K. Below $\omega \lesssim 500$ cm^{-1} a coupling of about $\lambda \simeq 0.5$ is required to obtain a reasonable fit to the infrared data (e.g., σ_s/σ_n); however, any attempt to increase the coupling in the low-frequency range (e.g., $\omega \lesssim 1500$ cm^{-1}) beyond this amount, leads to prominent features in the calculated spectra above 500 cm^{-1} that are not observed experimentally. The absence of these features in the infrared data may be interpreted as evidence against a conventional Eliashberg-like strong-coupling picture for the mechanism of superconductivity in $YBa_2Cu_3O_7$.

6. *Comparison with other techniques*

In studies of conventional superconductors, tunneling has generally been the technique which provided the most reliable information about the gap and coupling spectrum.[8] The high-temperature Cu-O superconductors have not yielded as easily to this technique[48-54] as many of the lower-T_c materials did. It has been suggested that the short coherence length intrinsically limits the ability of tunneling to probe the bulk properties of the high-T_c oxide superconductors.[47] Difficulties in producing an intrinsic surface at the junction interface may also add to these problems. In most of these studies, the surface of the superconductor acts as the insulating barrier in the measurements. Although tunnel junctions exhibiting ideal behavior have yet to be prepared from the Cu-O superconductors, gaplike features appearing at the superconducting transition are seen in many of the tunneling studies. The energy scales extracted from these measurements cover a fairly wide range but seem to be centered near $5-6kT_c$ for $YBa_2Cu_3O_7$.[48-54] This is smaller than the $7-8kT_c$ value obtained from the infrared measurements. In some tunneling studies corrections are made to account for a lower T_c at the junction surface than in the bulk of the material. These corrections tend to increase the estimates for $2\Delta/kT_c$, bringing them more in line with the infrared value. Anisotropy in the gap parallel and perpendicular to the planes has been reported by Tsai *et al.*[49] who finds an in-plane of $6kT_c$ and an out-of-plane gap of 3.5 kT_c. This anisotropy ratio (2:1) is roughly consistent with our infrared observations.[36] Given the presence of this large anisotropy, some of the quantitative differences between tunneling and infrared

could reflect the different way in which these probes average over the Fermi surface of an anisotropic superconductor. Kirtley[54] has recently proposed an interpretation of tunneling data in terms of gap anisotropy which is consistent with the (a-b)-plane and c-axis energy scales we find in the infrared. Also of interest is the recent report by Geerk *et al.*[53] in which the energy scale in the superconducting state shows very little temperature dependence as T approaches T (similar to our infrared results), although it should be pointed out that another group has reported a BCS temperature dependence in tunneling.[48]

Because of the large energy scales involved and improvements in resolution, the high-T_c cuprates are the first superconductors in which the energy gap is accessible to photoelectron spectroscopy. This technique is complementary to infrared in that it probes the single-particle density of states (which is gapped at Δ), rather than the conductivity (which is gapped at the pair-excitation threshold, 2Δ). Recent measurements of $Bi_2Sr_2CaCu_2O_{8-y}$ show a peak in the photoemission intensity and a corresponding shift of the photoemission threshold below T_c, from which a superconducting energy gap of $2\Delta \simeq 8kT_c$ is inferred.[55–57] These photoemission results confirm the importance of the $2\Delta_{a-b} \simeq 8kT_c$ energy scale originally inferred from infrared measurements of the a-b plane of high-quality $YBa_2Cu_3O_7$ crystals.[25,28,32,35,36] The agreement between careful photoemission and infrared measurements also appears to disprove the assertion that the gap cannot be seen in the infrared because of extreme cleanliness (see Appendix B).

Additional evidence for a redistribution of the electronic density of states at the superconducting transition is found in Raman-scattering experiments on both $YBa_2Cu_3O_7$ and $Bi_2Sr_2CaCu_2O_{8-y}$.[58–62] At T_c the electronic continuum scattering observed in these materials is depressed at low frequencies and develops a peak at higher frequency (near 400–500 cm^{-1}). If the high-frequency peak is interpreted as arising from excitations across the gap, a superconducting energy scale of about $7-8kT_c$ is inferred. These studies also report a continuum scattering below the peak in the superconducting state, which would not be expected in a conventional BCS superconductor.

A number of authors have reported estimates for the energy gap based on measurements of low-energy electromagnetic or thermodynamic properties. These properties, which include specific heat, nuclear relaxation, microwave absorption, and penetration depth, depend on the gap primarily through their dependence on the quasiparticle density at finite temperature in the superconducting state. Gap estimates from these quantities differ fundamentally from those of spectroscopic probes, in that they rely on theoretical fit to the temperature dependence of the data, rather than direct observation of quasiparticle excitations. Both Loram and Mirza[42] and Junod *et al.*[43,44] have noted that the specific-heat peak associated with the transition to superconductivity in $YBa_2Cu_3O_7$ is substantially narrower than the BCS result, and that the peak height is very large. These observations suggest a rate of decrease of entropy below T_c that far exceeds that in a mean-field (BCS) theory. Loram and Mirza[42] have shown that the width of this peak, and the drop in the electronic specific heat below the peak, can be fit using a gap of roughly twice the BCS value (i.e., $\sim 7kT_c$). In oxygen-reduced $YBa_2Cu_3O_{7-x}$ samples the specific-heat jump at T_c becomes difficult to observe or disappears completely.[44]

The study of nuclear resonance and the nuclear quadrupole relaxation rates has been one of the most intriguing and enigmatic subfields in high-T_c superconductivity.[63–69] In $YBa_2Cu_3O_y$, the relaxation rate for the plane Cu is substantially enhanced relative to both its Knight shift and the plane O rate, and deviates significantly from Korringa temperature dependence in the normal state. Both the oxygen and copper rates also fail to show evidence for an Hebel-Slichter peak below T_c, as predicted in the BCS theory. The absence of this peak may be related to either anisotropy in the gap or to the unconventional magnitude and temperature dependence of the gap, as discussed earlier. The inference of a characteristic energy scale from nuclear relaxation remains controversial because of the many unconventional aspects of the temperature dependence described above. In early work on the La site in $La_{2x}Sr_xCuO_4$ a gap of $2\Delta \simeq 8kT_c$ was reported,[63] and in work on $YBa_2Cu_3O_7$ (in which there was a problem with the site assignments) gaps of $2\Delta \simeq 8kT_c$ and $2\Delta \simeq 2kT_c$, associated with Cu chain and plane sites were proposed.[64] Recently Barrett *et al.*[69] have reported gap values of $(4-6)kT_c$ at the planes and $2kT_c$ for the chain site in $YBa_2Cu_3O_7$ based on Knight-shift data. In oxygen-deficient $YBa_2Cu_3O_{7-x}$, NQR observations have been interpreted as evidence for a magnetic gap which opens at temperatures well above T_c,[65] although other studies report that changes in the relaxation rate occur both at the higher temperatures and at T_c.[67]

7. *Comparison to* $Ba_{1-x}K_xBiO_3$ *and* $Bi_2Sr_2CaCu_2O_{8-y}$

It is interesting to compare the infrared data from the cubic oxide superconductor, $Ba_{0.6}K_{0.4}BiO_3$, with that from $YBa_2Cu_3O_7$. A more detailed presentation of normal- and superconducting-state infrared measurements of $Ba_{0.6}K_{0.4}BiO_3$ is given in Ref. 70. In Fig. 1 we have shown the ratio of the reflectivity in the superconducting state to that in the normal state for both $Ba_{0.6}K_{0.4}BiO_3$ and $YBa_2Cu_3O_7$. To facilitate a comparison, the reflectivity ratios are plotted as a function of frequency in units of kT_c for each superconductor. ($T_c \simeq 29$ K for $Ba_{0.6}K_{0.4}BiO_3$; $T_c \simeq 92$ K for $YBa_2Cu_3O_7$.) Qualitatively these data are very similar, however, from the frequency of the peak in R_s/R_n for $Ba_{0.6}K_{0.4}BiO_3$ an energy gap of about $2\Delta_c \simeq 4kT_c$ is obtained, while for $YBa_2Cu_3O_7$, on the other hand, an energy gap of $2\Delta_{a-b} \simeq 8kT_c$ is similarly inferred. This very large (a-b)-plane reduced energy gap lies well outside the conventional range, $2\Delta \simeq 3$ to $5kT_c$ in which previously studied superconductors (including $BaPb_{0.8}Bi_{0.2}O_3$ and $Ba_{0.6}K_{0.4}BiO_3$) have been found to lie.

We have also made infrared measurements of the (a-b)-plane reflectivity of the layered Cu-O superconductor $Bi_2Sr_2CaCu_2O_{8-y}$ ($T_c \simeq 80$ K). With this material the

reproducibility of the absolute reflectivity has not yet been obtained to our satisfaction, however, the reflectivity ratio, R_c/R_n shows a maximum at about 450 cm^{-1}. This result is analogous to our original result from $YBa_2Cu_3O_7$, and can be used to infer a characteristic energy scale of $2\Delta_{a-b} \simeq 8kT_c$ for $Bi_2Sr_2CaCu_2O_{8-y}$. The steplike drops in reflectivity at about 300 and 500 cm^{-1} reported by Reedyk *et al.*[87] are present in some of our spectra. An analysis of the temperature dependence of these features suggests that they may not be associated with the part of the sample which is metallic in the normal state and superconducting below T_c.

V. CONCLUSION

In this article our efforts to probe fundamental properties of the high-T_c cuprate superconductors by studying the temperature and frequency dependence of the infrared conductivity of $YBa_2Cu_3O_{7-x}$ are described. Although it is tempting to vary x and thus study this system over a wide range of parameter space, potential problems with electronic inhomogeneity, structural disorder, and reproducibility have discouraged us from emphasizing such an approach. Instead we have concentrated primarily on the reproducible properties of the stoichiometric high-T_c superconductor, $YBa_2Cu_3O_7$. While this limits the potential scope of our conclusions, it increases our confidence in the intrinsic value of the results.

We have reviewed what is known of the infrared properties of $YBa_2Cu_3O_7$, presented measurements of anisotropy both above and below T_c, and discussed possible implications of the normal-state data. Our analysis of the normal-state conductivity at low frequency leads to a frequency-dependent scattering rate of order $kT+\hbar\omega$, which may arise from an interaction of the carriers with a spin-related spectrum. As we have previously pointed out,[31] "the inelastic contribution to $\hbar/\tau^{*-1}(\omega)$ is of order $kT+\hbar\omega$, suggesting a nearly localized Fermi liquid, or that $YBa_2Cu_3O_7$ is at the edge of the regime in which a Fermi-liquid theory is well defined."[31] In the superconducting state, the salient feature of the infrared data appears to be the large energy gap observed in the (a-b)-plane response. Detailed temperature-dependent measurements establish a clear connection between this 500-cm^{-1} feature and the superconducting state (Figs. 6–8). At low temperature the data strongly suggests that this is the *intrinsic superconducting energy gap associated with the CuO_2 planes.* At finite temperatures unconventional or even exotic aspects of this gap feature emerge: (i) the transition to a nonsuperconducting state occurs at a temperature less than half that expected in mean-field theory, hence $2\Delta_{a-b} \simeq 8kT_c$, (ii) the energy of the gap seems to remain large up to as close to T_c as we can measure reliably, and (iii) evidence for possible fluctuations toward this gap may be present slightly (~ 10 K) above T_c. An understanding of these unusual phenomena may play a significant role in elucidating the underlying physics of the novel layered Cu-O superconductors.

ACKNOWLEDGMENTS

The authors acknowledge stimulating conversations with P. W. Anderson, N. E. Bickers, P. Coleman, H. Fukuyama, R. L. Greene, G. Gruner, P. M. Horn, J. R. Kirtley, K. Kitazawa, H. R. Krishnamurthy, A. P. Malozemoff, P. A. Lee, A. J. Millis, D. M. Newns, J. Orenstein, P. Pattnaik, K. F. Renk, T. M. Rice, D. J. Scalapino, A. J. Sievers, J. C. Soo, S. Tajima, and G. A. Thomas. Valuable technical assistance was received from J. Calise, G. Komsa, J. Sosik, R. Ruggiero, D. de Laura, and A. Davidson (Infrared Laboratories). We also thank K. F. Renk and J. Shutzmann for sharing their data and discussing their unpublished work on $YBa_2Cu_3O_7$ films.

APPENDIX A

It has been proposed that the 500-cm^{-1} gap which is prominent in the superconducting state is actually normal-state feature, which simply becomes exposed at low temperature in the superconducting state.[75]. Intrinsic to this suggestion is the belief that the conductivity is composed of a low-frequency Drude part, which collapses into a δ function at the superconducting transition, and a sequence of mid-infrared modes that account for the remaining conductivity. For the purpose of examining this proposal we adopt this point of view, which was previously considered in Sec. IV A, where such a deconstruction of $\sigma_{1n}(\omega)$ into such Drude and non-Drude parts was shown in Fig. 14.

Collapsing the entire Drude part of the conductivity into a δ function at the origin leaves the conductivity shown by the dotted curve in Figs. 14(a) and 14(b). It is this non-Drude part of the conductivity that is supposed to exhibit the 500-cm^{-1} gap in this approach. A fundamental problem with trying to construct the superconducting-state conductivity in this way is that the model conductivity (dotted curve) invariably returns to $\sigma_{1n}(\omega)$ much more slowly than the data, shown by the dashed curve in Fig. 14(b). [The rapid return of $\sigma_{1s}(\omega)$ to $\sigma_{1n}(\omega)$ at ~ 900 cm^{-1} is completely reproducible both in our data and that of Shutzman *et al.*[35].] This is the case with every (~ 50) parameter choice that we have tried. In order to generate a background conductivity that returned to $\sigma_{1n}(\omega)$ appropriately, one would require a Drude conductivity that vanishes abruptly between 500 and 800 cm^{-1}. This is not possible for any choice of parameters and presumably violates causality. As a related technical point, we further note that the observation that $\epsilon_{1s}(\omega)$ crosses above $\epsilon_{1n}(\omega)$ at about 550 cm^{-1} [Fig. 5(c)] cannot be reproduced in a model that collapses the entire Drude part of $\sigma_{1n}(\omega)$ into a δ function.

In summary, collapsing all of the free-carrier conductivity into the δ function would cause changes in $\sigma_1(\omega)$ to occur at much higher frequency seen in the data. One is therefore forced by the data to leave the conductivity above 500 cm^{-1} substantially unchanged, while collapsing most of the lower-frequency conductivity into a δ function at $\omega=0$ below T_c. This is the signature of a superconducting energy gap.

APPENDIX B

As shown, for example, in Figs. 6 and 8, the superconducting-state conductivity exhibits a threshold (rapid onset of absorption) at about 500 cm^{-1}. It is quite natural to associate this 500-cm^{-1} threshold with a superconducting energy gap in the free-carrier conductivity. It has been suggested that $YBa_2Cu_3O_7$ is so clean, however, that one should not be able to see this energy gap in an infrared measurement. This is ultimately a quantitative rather than a qualitative question [the gap does not disappear abruptly as one passes from dirty ($l/\xi_0 < 1$) to clean ($l/\xi_0 > 1$).] In this Appendix we discuss both the assessment of the degree of cleanliness of $YBa_2Cu_3O_7$, and the question of whether or not one should see a gap. This discussion, if necessity, predicated on the assumption that the low-frequency normal-state conductivity of $YBa_2Cu_3O_7$ can be described in a more or less conventional way, which may not be justified. While we have taken the space to respond to this issue here, it is fair to say that we feel more comfortable describing what the data does show (see, e.g., Figs. 5–8), rather than arguing about what one should be able to see.

The clean limit is usually defined by the inequality $l \gg \xi$, where l is the mean-free path and ξ is the coherence length. An equivalent definition in terms of characteristic frequencies instead of lengths is $\pi\Delta\tau^* \gg 1$, where 2Δ is the superconducting energy gap and τ^{*-1} is the (renormalized) low-frequency scattering rate [i.e., the width of the (Drude) conductivity peak at low ω]. In the following calculations we have used the Eliashberg equations[92] with a fixed normal-state carrier density and superconducting energy gap. We have varied the scattering rate, τ^{*-1}, and calculated the conductivity in the normal and superconducting state.

In examining this issue we have found that the degree of cleanliness, as quantified by l/ξ_0 or $\pi\Delta\tau^*$, is not really the correct measure of how difficult it is to see the gap in this model. Although it is true that for fixed 2Δ the gap becomes increasingly more difficult to see as τ^* decreases, it is not true that for fixed τ^{*-1} that the gap becomes more difficult to observe as 2Δ increases. This is a consequence of the fact that the noise in $\sigma_1(\omega)$ grows like $1/\omega^2$ in a clean system, thus offsetting the corresponding $1/\omega^2$ increase in $\sigma_1(\omega)$. One thus finds that in a system with a uniform level of noise in the reflectivity, that the level to which that noise must be reduced in order see the gap is independent of the magnitude of 2Δ. In fact the parameter that determines how difficult it is to see the gap is τ^{*-1}/ω_p. This result becomes intuitively obvious when one realizes that in a clean system the difference between the reflectivity and unity is proportional to τ^{*-1}/ω_p and independent of frequency. In the following we continue to examine the question of how clean $YBa_2Cu_3O_7$ is and whether or not one should be able to see the gap; however, it is noted that the mathematics surrounding this issue are a bit more complicated than the statement that "in a clean superconductor you can't see the gap" would lead one to believe.

For a superconductor in the extreme clean limit 2Δ is much much greater than τ^{*-1}. In this case, which is shown in Fig. 16(a), virtually all of the area in $\sigma_1(\omega)$ goes into the δ function at $\omega=0$ in the superconducting state. The magnitude of $\sigma_1(\omega)$ at 2Δ is so small that the gap may not be readily observable. In the moderately clean case most of the area in $\sigma_1(\omega)$ still goes into the δ function, however, there is now sufficient conductivity at $\omega=2\Delta$ to make the gap observable as shown in Fig. 16(b). In the dirty limit, shown in Fig. 16(c), the conductivity is essentially constant from dc up to 2Δ, and only a small fraction of the total area in $\sigma_1(\omega)$ goes into the δ function at $\omega=0$. In this case [Fig. 16(c)] the superfluid density is much smaller, and the penetration depth much larger than in either of the clean cases [Figs. 16(a) and 16(b)] (even though the normal-state carrier density is the same for all three cases). As an aside, we note that while conductivity sum-rule related arguments can be used to separate the dirty and clean limits, they will not generally allow a distinction to be made between the extremely and moderately clean cases [Figs. 16(a) and 16(b)].

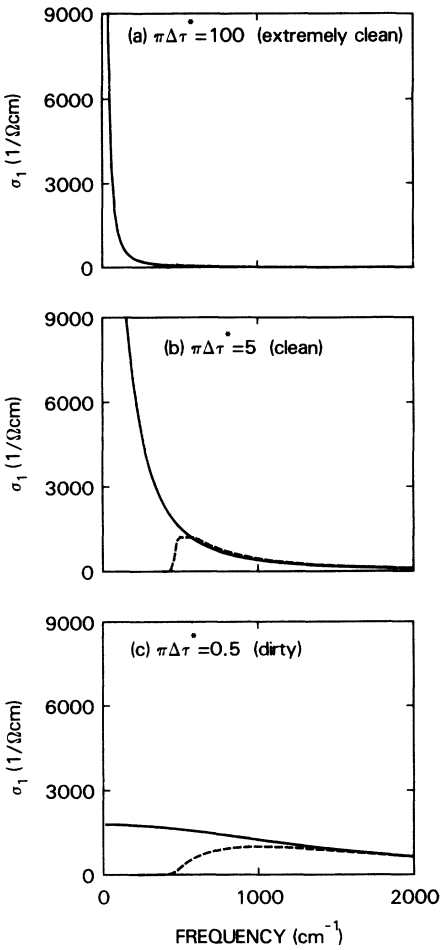

FIG. 16. Calculated conductivities of a model superconductor for several values of the scattering rate τ^{*-1} are shown. Note that τ^{*-1} is the width of peak in $\sigma_{1n}(\omega)$ (solid lines), and that $\pi\Delta\tau^*=l/\xi_0$ in a conventional superconductor. The total area in $\sigma_{1n}(\omega)$ and the gap ($2\Delta=500$ cm^{-1}) are the same in each case, while τ^{*-1} is varied as shown. Near T_c, $YBa_2Cu_3O_7$ falls into the intermediate (moderately clean) case, shown in (b), although it should be noted that the normal-state conductivity does not actually follow a Drude form.

In $YBa_2Cu_3O_7$ characteristic features of the supercon-

ducting state are fully developed by 50 K and are well developed even at temperatures as high as 80 K (Fig. 6). In this temperature range near T_c, we use the normal-state conductivity just above T_c to estimate approximately how "clean" $YBa_2Cu_3O_7$ is. The width of the conductivity peak is about 150 cm^{-1} at $T=100$ K, thus for a 500-cm^{-1} gap one obtains $\pi\Delta\tau^* \simeq 5$, which corresponds to Fig. 16(b). Looking in more detail, with a dc conductivity of 20 000 $(\Omega^{-1}\,cm)^{-1}$ (i.e., $\rho=50$ $\mu\Omega$ cm), this implies a conductivity of about 2000 $(\Omega^{-1}\,cm)^{-1}$ at 500 cm^{-1} ($\sim 8kT_c$), which is clearly adequate to see the gap (see, e.g., Fig. 6). These values indicate that at $T \simeq 100$ K the conductivity of $YBa_2Cu_3O_7$ is consistent with the intermediate case [Fig 16(b)], in which there is sufficient conductivity at 2Δ to observe a gap in $\sigma_1(\omega)$.

Some of the claims that $YBa_2Cu_3O_7$ is too clean to see the gap are based on hypothetical extrapolations of the normal-state data to $T=0$. These extrapolations are quite speculative and should be examined closely, especially since they lead to results that seem to contradict the infrared data at intermediate temperatures (e.g., 50 K), where, as noted above, the 500-cm^{-1} gap is quite well developed.

[1]R. E. Glover and M. Tinkham, Phys. Rev. **104**, 844 (1956); **108**, 243 (1957).

[2]I. Giaver, Phys. Rev. Lett. **5**, 464 (1960).

[3]D. M. Ginsberg and M. Tinkham, Phys. Rev. **118**, 990 (1960).

[4]P. L. Richards and M. Tinkham, Phys. Rev. **119**, 575 (1960).

[5]M. Tinkham, in *Far Infrared Properties of Solids,* edited by S. S. Mitra and S. Nudelman (Plenum, New York, 1970).

[6]R. R. Joyce and P. L. Richards, Phys. Rev. Lett. **24**, 1007 (1970).

[7]G. Brandli and A. J. Sievers, Phys. Rev. B **5**, 3550 (1972).

[8]W. L. McMillan and J. M. Rowell, in *Superconductivity,* edited by R. D. Parks (Marcel-Dekker, New York, 1969).

[9]J. G. Bednorz, and K. A. Müller, Z. Phys. B **64**, 189 (1986).

[10]M. K. Wu, J. Ashburn, C. J. Torng, P. H. Hor, R. L. Meng, L. Gao, Z. J. Huang, Y. Q. Wang, and C. W. Chu, Phys. Rev. Lett. **58**, 908 (1987).

[11]P. E. Sulewski, A. J. Sievers, R. A. Buhrman, J. M. Tarascon, and L. H. Greene, Phys. Rev. B **35**, 5330 (1987).

[12]Z. Schlesinger, R. L. Greene, J. G. Bednorz, and K. A. Müller, Phys. Rev. B **35**, 5334 (1987).

[13]U. Walter, M. S. Sherwin, A. Stacy, P. L. Richards, and A. Zettle, Phys. Rev. B **35**, 5327 (1987).

[14]J. R. Kirtley, R. T. Collins, Z. Schlesinger, W. J. Gallagher, R. L. Sandstrom, T. R. Dinger, and D. A. Chance, Phys. Rev. B **35**, 8846 (1987).

[15]R. T. Collins, Z. Schlesinger, R. H. Koch, R. B. Laibowitz, T. S. Plaskett, P. Freitas, W. J. Gallagher, R. L. Sandstrom, and T. R. Dinger, Phys. Rev. Lett. **59**, 704 (1987).

[16]D. A. Bonn, A. H. O'Reilly, J. E. Greedan, C. V. Stager, T. Timusk, K. Karamus, and D. B. Tanner, Phys. Rev. B **37**, 1574 (1988).

[17]L. Genzel, A. Wittlin, M. Bauer, M. Cardona, E. Schönherr, and A. Simon, Phys. Rev. B **40**, 2170 (1989).

[18]J. Orenstein, G. A. Thomas, D. H. Rapkine, C. G. Bethea, B. F. Levine, R. J. Cava, E. A. Rietman, and D. W. Johnson, Jr., Phys. Rev. B **36**, 729 (1987).

[19]K. Kamaras, C. D. Porter, M. G. Doss, S. L. Herr, D. B. Tanner, D. A. Bonn, J. E. Greedan, A. H. O'Reilly, C. V. Stager, and T. Timusk, Phys. Rev. B **36**, 733 (1987).

[20]K. Kamaras, C. D. Porter, M. G. Doss, S. L. Herr, D. B. Tanner, D. A. Bonn, J. E. Greedan, A. H. O'Reilly, C. V. Stager, and T. Timusk, Phys. Rev. Lett. **59**, 919 (1987).

[21]P. E. Sulewski, T. W. Noh, J. T. McWhirter, and A. J. Sievers, S. E. Russek, R. A. Buhrman, C. S. Jee, J. E. Crow, R. E. Salomon, and G. Meyer, Phys. Rev. B **36**, 2357 (1987).

[22]Z. Schlesinger, R. T. Collins, M. W. Shafer, and E. M. Engler, Phys. Rev. B **36**, 5275 (1987).

[23]J. Orenstein and D. H. Rapkine, Phys. Rev. Lett. **60**, 968 (1988).

[24]K. Kamaras, C. D. Porter, M. G. Doss, S. L. Herr, D. B. Tanner, D. A. Bonn, J. E. Greedan, A. H. O'Reilly, C. V. Stager, and T. Timusk, Phys. Rev. Lett. **60**, 969 (1988).

[25]Z. Schlesinger, R. T. Collins, D. L. Kaiser, and F. Holtzberg, Phys. Rev. Lett. **59**, 1958 (1987).

[26]I. Bozovic, D. Kirillov, A. Kapitulnik, K. Char, M. R. Hahn, M. R. Beasley, T. H. Geballe, Y. H. Kim, and A. J. Heeger, Phys. Rev. Lett. **59**, 2219 (1987).

[27]S. Tajima, S. Uchida, H. Ishii, H. Takagi, S. Tanaka, U. Kawabe, H. Hasegawa, T. Aita, and T. Ishiba, Mod. Phys. Lett. B **1**, 353 (1988).

[28]Z. Schlesinger, R. T. Collins, D. L. Kaiser, F. Holtzberg, G. V. Chandrashekar, M. W. Shafer, and T. M. Plaskett, Physica C **153**, 1734 (1988).

[29]T. Timusk, S. L. Herr, K. Kamarás, C. D. Porter, D. B. Tanner, D. A. Bonn, J. D. Garrett, C. V. Stager, J. E. Greedan, and M. Reedyk, Phys. Rev. B **38**, 6683 (1988).

[30]G. A. Thomas, J. Orenstein, D. H. Rapkine, M. Capizzi, A. J. Millis, R. N. Bhatt, L. F. Schneemeyer, and J. V. Waszczak, Phys. Rev. Lett. **61**, 1313 (1988).

[31]R. T. Collins, Z. Schlesinger, F. Holtzberg, P. Chaudari, and C. Field, Phys. Rev. B **39**, 6571 (1989).

[32]T. W. Noh, P. E. Seluski, S. Kaplan and A. J. Sievers, D. K. Lanthrop and R. A. Burham, Mater. Res. Soc. Symp. Proc. **99**, 435 (1988).

[33]M. Suzuki, Phys. Rev. B **39**, 2312 (1989).

[34]S. Tajima, H. Ishii, T. Nakahashi, T. Takagi, S. Uchida, M. Seki, S. Suga, Y. Hidaka, M. Suzuki, T. Murakami, K. Oka, and H. Unoki, J. Opt. Soc. Am. B **6**, 475 (1989).

[35]J. Schutzmann, W. Ose, J. Keller, K. F. Renk, B. Roas, L. Schulz and G. Saemann-Ischenko, Europhys. Lett. **8**, 679 (1989).

[36]R. T. Collins, Z. Schlesinger, F. Holtzberg, and C. Field, Phys. Rev. Lett. **63**, 422 (1989).

[37]B. Koch, H. P. Geserich and Th. Wolf, Solid State Commun. (to be published).

[38]S. Uchida, H. Takagi, and Y. Tokura, Physica C **162-164**, 1677 (1989).

[39]R. T. Collins, *et al.* (unpublished).

[40]A. T. Forrester, Phys. Rev. B **110**, 776 (1958).

[41]M. Tinkham and R. E. Glover, Phys. Rev. B **110**, 778 (1958).

[42]J. W. Loram and K. A. Mirza, Physica C **153-155**, 1020 (1988).

[43]A. Junod, A. Bezinge, and J. Muller, Physica C **152**, 50 (1988).

[44]A. Junod, A. Bezinge, D. Eckert, T. Graf, and J. Muller, Physica C **152**, 495 (1988); A. Junod, D. Eckert, T. Graf, G. Triscone, and J. Muller, Physica C **162-164**, 482 (1989).

[45]L. Krusin-Elbaum, R. L. Greene, F. Holzberg, A. P. Malozemoff, and Y. Yeshurun, Phys. Rev. Lett. **62**, 217 (1989).
[46]D. R. Harshman *et al.*, Phys. Rev. B **39**, 851 (1989).
[47]G. Deutscher and K. A. Müller, Phys. Rev. Lett. **59**, 1745 (1987).
[48]M. Lee, A. Kapitulnik, and M. R. Beasley, *Proceedings of the NEC Symposium on Mechanisms of High-Temperature Superconductivity, Tokyo, Japan, 1988,* edited by H. Kamimura and A. Oshiyama (Springer-Verlag, Berlin, 1989).
[49]J. S. Tsai, I. Takeuchi, J. Fujita, T. Yoshitake, S. Miura, S. Tanaka, T. Terashima, Y. Bando, K. Iijima, and K. Yamamoto, Physica C **153**, 1385 (1988).
[50]K. E. Gray, M. E. Hawley, and E. R. Moog, in *Novel Mechanisms of Superconductivity,* edited by S. A. Wolf and V. Z. Kreslin (Plenum, New York, 1987), p. 611.
[51]A. Barone, Physica C **153-155**, 1712 (1988).
[52]M. Gurvitch, J. M. Valles, Jr., A. M. Cucolo, R. C. Dynes, J. P. Garno, L. F. Schneemeyer, and J. V. Waszczak, Phys. Rev. Lett. **63**, 1008 (1989).
[53]J. Geerk, X. X. Xi, and G. Linker, Z. Phys. B **73**, 329 (1988).
[54]J. R. Kirtley, Int. J. Mod. Phys. B (to be published).
[55]R. Manzke, T. Buslaps, R. Classen, and J. Fink, Europhys. Lett. **9**, 477 (1989).
[56]J.-M. Imer, F. Patthey, B. Dardel, W.-D. Schneider, Y. Baer, Y. Petroff, and A. Zettl, Phys. Rev. Lett. **62**, 336 (1989).
[57]C. G. Olson, R. Liu, A.-B. Yang, D. W. Lynch, A. J. Arko, R. S. List, B. W. Veal, Y. C. Chang, P. Z. Jiang, and A. P. Paulikas, Science **245**, 731 (1989).
[58]K. B. Lyons, S. H. Liou, M. Hong, H. S. Chen, J. Kwo, and T. J. Negran, Phys. Rev. B **36**, 5592 (1987).
[59]S. L. Cooper, M. V. Klein, B. G. Pazol, J. P. Rice, and D. M. Ginzberg, Phys. Rev. B **37**, 5920 (1988); S. L. Cooper, F. Slakey, M. V. Klein, J. P. Rice, E. D. Bukowski, and D. M. Ginsberg, *ibid.* **38**, 11 934 (1988).
[60]A. Yamanaka, T. Kimura, F. Minami, K. Inque, and S. Takekawa, J. Appl. Phys. **27**, L1902 (1988).
[61]D. Kirillov, I. Bozovic, T. H. Geballe, A. Kapitulnik, and D. B. Mitzi, Phys. Rev. B **38**, 11 955 (1988).
[62]C. Thomsen and M. Cardona, in *Physical Properties of High-Temperature Superconductors,* edited by D. M. Ginsberg (World Scientific, Singapore, 1989).
[63]H. Seidel, F. Hentsch, M. Mehring, J. G. Bednorz, and K. A. Müller, Europhys. Lett. **5**, 647 (1988).
[64]W. W. Warren, Jr., R. E. Walstedt, G. F. Brennert, G. P. Espinosa, and J. P. Remeika, Phys. Rev. Lett. **59**, 1860 (1987). The Cu site assignments in this paper are incorrect and should be reversed.
[65]W. W. Warren, Jr., R. E. Walstedt, G. F. Bennert, R. J. Cava, R. Tycko, R. F. Bell, and G. Dabbagh, Phys. Rev. Lett. **62**, 1193 (1989).
[66]M. Takigawa, P. C. Hammel, R. H. Heffner, and Z. Fisk, Phys. Rev. B **39**, 7371 (1989).
[67]T. Imai, T. Shimizu, H. Ysuoka, Y. Ueda, K. Yosimura, and K. Kosuge, Phys. Rev. B (to be published).
[68]P. C. Hammel, M. Takigawa, R. H. Heffner, Z. Fisk, and K. C. Ott, Phys. Rev. Lett. **63**, 1992 (1989).
[69]S. E. Barrett, D. J. Durand, C. H. Pennington, C. P. Slichter, T. A. Freidmann, J. P. Rice, and D. M. Ginsberg, Phys. Rev. B **41**, 6283 (1990).
[70]Z. Schlesinger, R. T. Collins, J. A. Calise, D. J. Hinks, A. W. Mitchell, Y. Zheng, B. Dabrowski, N. E. Bickers, and D. J. Scalapino, Phys. Rev. B **40**, 6862 (1989).
[71]D. L. Kaiser, F. Holtzberg, B. A. Scott, and T. A. McGuire, Appl. Phys. Lett. **51**, 1040 (1987).
[72]G. Koren, A. Gupta, E. A. Giess, A. Segmuller, and R. B. Laibowitz, Appl. Phys. Lett. **54**, 1054 (1989).
[73]G. Koren, A. Gupta, and R. J. Baseman, Appl. Phys. Lett. **54**, 1920 (1989).
[74]F. Wooten, *Optical Properties of Solids* (Academic, San Francisco, 1972).
[75]G. A. Thomas and J. Orenstein (private communication).
[76]K. Kamaras, S. L. Herr, C. D. Porter, N. Tache, D. B. Tanner, S. Etamad, T. Venkatesan, E. Chase, A. Inam, X. D. Wu, M. S. Hegde, and B. Dutta (unpublished).
[77]I. Bozovic, K. Char, S. J. B. Yoo, A. Kapitulnik, M. R. Beasley, T. H. Geballe, Z. Z. Wang, S. Hagen, N. P. Ong, D. E. Aspnes, and M. K. Kelly, Phys. Rev. B **38**, 5077 (1988).
[78]T. W. Noh, S. G. Kaplan, and A. J. Sievers, Phys. Rev. Lett. **62**, 599 (1989).
[79]M. W. Shafer, T. Penney, and B. L. Olson, Phys. Rev. B **36**, 4047 (1987); M. W. Shafer, T. Penney and B. L. Olson, R. L. Greene, and R. H. Koch, *ibid.* **39**, 2914 (1989).
[80]J. Clayhold, N. P. Ong, Z. Z. Wang, J. M. Tarascon, and T. Barboux, Phys. Rev. B **39**, 7324 (1989).
[81]Y. Tokura, J. B. Torrance, T. C. Huang, and A. I. Nazzal, Phys. Rev. B **38**, 7156 (1988).
[82]W. F. Brinkman and T. M. Rice, Phys. Rev. B **2**, 1234 (1970).
[83]P. W. Anderson, Science **235**, 1196 (1987); P. W. Anderson and Z. Zou, Phys. Rev. Lett. **60**, 132 (1988).
[84]F. E. Pinkerton, B. C. Webb, A. J. Sievers, J. W. Wilkins, and L. J. Sham, Phys. Rev. Lett. **57**, 1951 (1986).
[85]B. C. Webb, A. J. Sievers, and T. Mahahlisin, Phys. Rev. Lett. **57**, 1951 (1986).
[86]P. E. Sulewski, A. J. Sievers, M. B. Maple, M. S. Torikachvili, J. L. Smith, and Z. Fisk, Phys. Rev. B **38**, 5338 (1988).
[87]M. Reedyk, D. A. Bonn, J. D. Garrett, J. E. Greedan, C. V. Stager, T. Timusk, K. Kamarás, and D. B. Tanner, Phys. Rev. B **38**, 11 981 (1988); D. A. Bonn (private communication).
[88]S. Schmitt-Rink, C. M. Varma, and A. E. Ruckenstein, Phys. Rev. Lett. **60**, 2793 (1988).
[89]T. M. Rice and F. C. Zhang, Phys. Rev. B **39**, 815 (1989).
[90]C. L. Kane, P. A. Lee, and N. Read, Phys. Rev. B **39**, 6880 (1989).
[91]M. Schluter (private communication).
[92]N. E. Bickers, D. J. Scalapino, R. T. Collins, and Z. Schlesinger, Phys. Rev. B (to be published).
[93]P. W. Anderson, J. Chem. Solids **11**, 26 (1959); P. L. Richards, Phys. Rev. Lett. **7**, 412 (1961).
[94]T. Schneider, H. De Raedt, and M. Frick (unpublished).
[95]K. F. Renk (private communication).
[96]L. Drabeck, G. Gruner, J-J. Chang, A. Inam, X. D. Wu, L. Nazar, T. Venkatesan, and D. J. Scalapino, Phys. Rev. B **40**, 7350 (1989).
[97]D. W. Cooke *et al.* (unpublished).
[98]P. P. Freitas, C. C. Tsuei, and T. S Plaskett, Phys. Rev. B **36**, 833 (1987).
[99]B. Oh, K. Char, A. D. Kent, M. Naito, M. R. Beasley, T. H. Geballe, R. H. Hammond, A. Kapitulnik, and J. M. Graybeal, Phys. Rev. B **37**, 7861 (1988).
[100]S. J. Hagen, Z. Z. Wang, and N. P. Ong, Phys. Rev. B **38**, 7137 (1988).
[101]S. E. Inderhees, M. B. Salamon, N. Goldenfield, J. P. Rice, B. G. Pazol, D. M. Ginsberg, J. Z. Liu, and G. W. Crabtree, Phys. Rev. Lett. **60**, 1178 (1988).
[102]W. C. Lee, R. A. Klemm, and D. C. Johnston, Phys. Rev. Lett. **63**, 1012 (1989).